Supplementary Information

Ladderization of polycyclic aromatic hydrocarbons enhances electrical conductivity through additional coherent channels

Qing Wang,a,# Na Huang,a,b,e,# Ruiying Zhang,a Li-Chuan Chen,c Jianfeng Yan,a Zhong-Ning Chen,b Yuanming Li,a,* Qian-Chong Zhangb,d,*

1.Key Laboratory of Advanced Carbon-Based Functional Materials (Fujian Province University), College of Chemistry, Fuzhou University, Fuzhou, 350108, China. Email: yuanming.li@fzu.edu.cn

2. State Key Laboratory of Structural Chemistry, Fujian Institute of Research on the Structure of Matter, Chinese Academy of Sciences, Fuzhou, Fujian 350002, China. Email: zhangqianchong@fjirsm.ac.cn

3. Institute of Modern Optics and Center of Single-Molecule Science, Tianjin Key Laboratory of Micro-scale Optical Information Science and Technology, Nankai University, Tianjin, 300350, China

# These authors contributed equally to this work

E-mail: zhangqianchong@fjirsm.ac.cn

Table of Contents

1. General

All reagents and solvents were obtained from commercial suppliers and used without further purification unless noted otherwise. The silica-gel column chromatography was performed using silica gel (200–300 mesh). All reactions were run under argon atmosphere unless otherwise stated. Nuclear magnetic resonance (NMR) spectra were recorded on a JEOL JNM-ECZ500R (^{1}H 600 MHz, ^{13}C 151 MHz) spectrometer. Chemical shifts are expressed in parts per million (ppm) relative to tetramethylsilane (δ 0.00 ppm). ^{1}H and ^{13}C NMR spectra are referenced against the residual solvent peak ($CDCl_3$ δ_H = 7.26 ppm, $CDCl_3$ δ_C = 77.16 ppm). The high-resolution mass spectra (HRMS) were conducted on Thermo fisher scientific exactive plus LC-MS (ESI) mass spectrometer. UV-vis-NIR spectra were recorded on SHIMADZU UV-2700 spectrophotometer in dichloromethane.

2. Synthetic procedures

2.1 Synthesis of 2

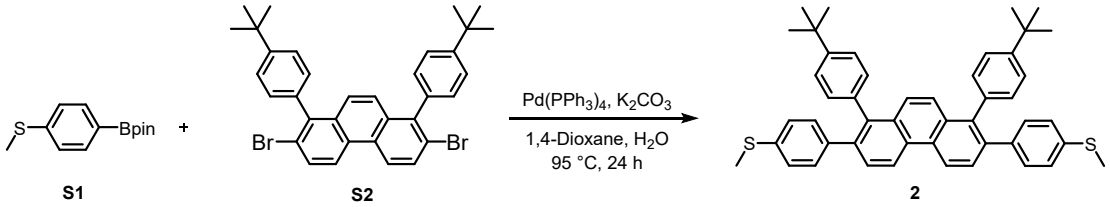

Scheme S1. Synthetic Route of **2**

Compound s2: **s2** was prepared according to previous literature.[1]

Compound 2: Compound **s2** (150 mg, 0.25 mmol, 1.00 equiv.), compound **s1** (250 mg, 1 mmol, 4.00 equiv.), $Pd(PPh_3)_4$ (43 mg, 0.0375 mmol, 0.15 equiv.) and K_2CO_3 (173 mg, 1.25 mmol, 5.00 equiv.) were added to a 25 mL round-bottom flask equipped with a stir bar. After the flask was evacuated and refilled with argon 3 times, degassed 1,4-dioxane (7.0 mL) and water (1.0 mL) were transferred to the flask via syringe. The mixture was stirred at 95 °C for 24 h. After cooling down to room temperature, the aqueous layer was extracted with dichloromethane (DCM) (25 mL) for three times. The combined organic layers were washed with brine and dried with Na_2SO_4, filtered and concentrated under reduced pressure. The residue was then purified by silica gel column chromatography with petroleum ether/DCM (20:1 → 3:1, v/v) as eluent to give the compound **2** (160 mg, 0.021 mmol, 93%) as a white powder solid. ^{1}HNMR (600 MHz, $CDCl_3$) δ 8.82 (d, J = 8.7 Hz, 2H), 7.73 (d, J = 8.5 Hz, 2H), 7.53 (s, 2H), 7.34–7.28 (d, 4H), 7.20–7.02 (m, 12H), 2.46 (s, 6H), 1.32 (s, 18H). ^{13}C NMR (151 MHz, $CDCl_3$) δ 149.6, 138.7, 138.4, 138.3, 136.1, 135.9, 131.0, 130.7, 130.5, 129.4, 128.5, 125.6, 125.4, 124.7, 122.2, 34.4, 31.3, 15.7. HRMS analysis (ESI): calculated for $C_{48}H_{46}S_2$ $[M+H]^+$: 687.3114, found: 687.3102.

2.2 Synthesis of 2TP

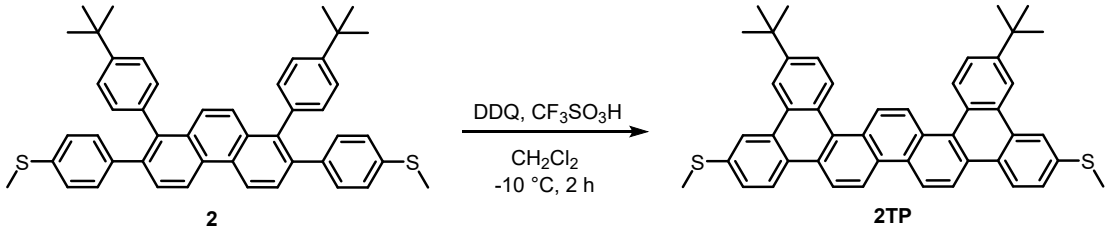

Scheme S2. Synthetic Route of **2TP**

Compound 2TP: A 100 mL Schlenk flask charged with the Compound **2** (21 mg, 0.03 mmol, 1.00 equiv.), and 2,3-dichloro-5,6-dicyano-1,4-benzoquinone (DDQ) (16 mg, 0.072 mmol, 2.40 equiv.) was purged with argon for ten minutes. Dry DCM (30 mL) was added to make a clear solution. The mixture was then cooled down to –10°C under argon atmosphere. After stirring at –10 °C for 15 minutes, TfOH (0.3 mL) was added at –10 °C. The mixture immediately turned black upon the addition of TfOH. The mixture was stirred at –10°C for 2 h and then quenched by pouring it into sat. aq. $NaHCO_3$ (10 mL). After stirring vigorously for 15 minutes, the aqueous layer was extracted with DCM (30 mL) for three times. The combined organic layers were washed with brine and dried with Na_2SO_4, filtered and concentrated under reduced pressure. the crude product mixture was purified by silica gel column chromatography (DCM/petroleum = 1/20 to 1/2, v/v) gave **2TP**, then recrystallization from $CHCl_3$/ CH_3OH, and drying in vacuum as a white solid (9 mg, 0.12 mmol, 43%). ^{1}H NMR (600 MHz, $CDCl_3$) δ 9.03 (dd, *J* = 15.5, 8.8 Hz, 4H), 8.87 (s, 2H), 8.80 (d, *J* = 9.1 Hz, 2H), 8.71–8.65 (m, 4H), 8.60 (d, *J* = 2.0 Hz, 2H), 7.85 (dd, *J* = 8.6, 2.0 Hz, 2H), 7.65 (dd, *J* = 8.6, 1.9 Hz, 2H), 2.73 (s, 6H), 1.58 (s, 18H). ^{13}C NMR (151 MHz, Tetrachloroethan-d2) δ 150.2, 137.7, 130.8, 130.2, 129.9, 128.3, 128.1, 127.8, 127.4, 126.4, 126.0, 125.0, 124.6, 123.7, 122.4, 121.3, 120.7, 120.5, 119.5, 74.2, 35.3, 31.7, 29.9. HRMS analysis (ESI): calculated for $C_{48}H_{42}S_2$ $[M+H]^+$: 683.2801, found: 683.2801.

2.3 Synthesis of TP

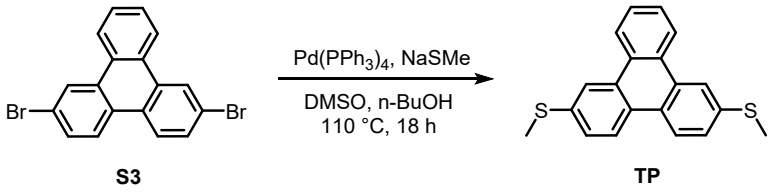

Scheme S3. Synthetic Route of **TP**

Compound TP: A 50 mL Schlenk flask charged with the Compound **S3** (58 mg, 0.15 mmol) and NaSMe (105 mg, 1.5 mmol, 10.00 equiv.) were added under a positive pressure of nitrogen, then DMSO (6 mL), *n*-BuOH (6 mL) and $Pd(PPh_3)_4$ (17 mg, 0.148 mmol, 0.10 equiv.) were added, and the suspension was heated to 110 °C in an oil bath for 18 hours. After cooling down to room temperature, the aqueous layer was extracted with dichloromethane (DCM) for three times. The combined organic layers were washed with brine and dried with Na_2SO_4, filtered and concentrated under reduced pressure. The residue was then purified by silica gel column chromatography with (petroleum ether/DCM/ = 50/1 to petroleum ether/DCM = 10/1, v/v) afforded the compound **TP** (36 mg, 0.11 mmol, 75%) as a white powder solid. HRMS analysis (ESI): calculated for $C_{20}H_{16}S_2$ [M]+: 320.0688, found: 320.0682.

^1H NMR and ^{13}C NMR of **TP** are published in the literature.[2]

2.4 Synthesis of 2TP-Core

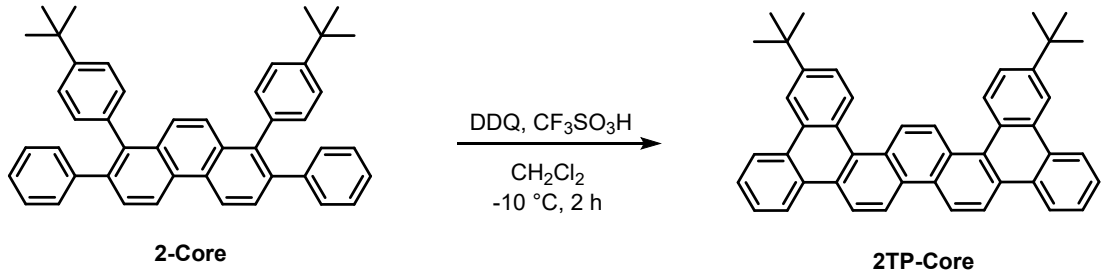

2-Core **2TP-Core**

Compound 2TP-Core: 100 mL Schlenk flask charged with the Compound **2-Core** (18 mg, 0.03 mmol, 1.00 equiv.), and 2,3-dichloro-5,6-dicyano-1,4-benzoquinone (DDQ) (16 mg, 0.072 mmol, 2.40 equiv.) was purged with argon for ten minutes. Dry DCM (30 mL) was added to make a clear solution. The mixture was then cooled down to –10°C under argon atmosphere. After stirring at –10 °C for 15 minutes, TfOH (0.6 mL) was added at –10 °C. The mixture immediately turned black upon the addition of TfOH. The mixture was stirred at –10°C for 2 h and then quenched by pouring it into sat. aq. $NaHCO_3$ (10 mL). After stirring vigorously for 15 minutes, the aqueous layer was extracted with DCM (30 mL) for three times. The combined organic layers were washed with brine and dried with Na_2SO_4, filtered and concentrated under reduced pressure. the crude product mixture was purified by silica gel column chromatography (DCM/petroleum = 1/20 to 1/2, v/v) gave **2TP-Core**, then recrystallization from $CHCl_3$/ CH_3OH, and drying in vacuum as a white solid (6 mg, 0.11 mmol, 35%). ^{1}H NMR (600 MHz, $CDCl_3$) δ 9.06 (t, J = 8.8 Hz, 4H), 8.93–8.86 (m, 4H), 8.77 (d, J = 4.4 Hz, 6H), 7.85 (dd, J = 8.3, 2.0 Hz, 2H), 7.78–7.71 (m, 4H), 1.59 (s, 18H). ^{13}C NMR (151 MHz, Tetrachloroethane-d_2) δ 150.31, 130.86, 130.57, 130.29, 130.12, 130.00, 128.58, 128.52, 128.44, 127.82, 127.56, 126.65, 124.92, 124.20, 123.50, 122.59, 121.74, 119.83, 35.47, 31.89.

3. X-Ray Crystallography

3.1 Experimental details on crystal growth

Single crystals of **2** (Colorless transparent needle) obtained by slowly evaporating Toluene-MeOH (1:3, v/v) solution at room temperature.

Table S1. Crystallographic data and structure refinement details for **2**.

Compound	**2**
CCDC Deposition number	2525092
Empirical formula	$C_{55}H_{54}S_2$
Formula weight	779.10
Temperature/K	100.4(9)
Crystal system	monoclinic
Space group	P21/n
a/Å	8.53820(10)
b/Å	22.3478(3)
c/Å	22.2413(3)
α/°	90
β/°	90.8700(10)
γ/°	90
Volume/Å3	4243.37(9)
Z	4
ρcalcg/cm3	1.220
μ/mm-1	0.920
F(000)	1664.0
Crystal size/mm3	0.21 × 0.06 × 0.05
Radiation	micro-focus metaljet (λ = 1.3405)
2Θ range for data collection/°	4.874 to 110.748
Index ranges	-10 ≤ h ≤ 8, -27 ≤ k ≤ 26, -27 ≤ l ≤ 26
Reflections collected	28383
Independent reflections	8062 [Rint = 0.0412, Rsigma = 0.0404]
Data/restraints/parameters	8062/399/619
Goodness-of-fit on F2	1.059
Final R indexes [I>=2σ (I)]	R1 = 0.0405, wR2 = 0.1066
Final R indexes [all data]	R1 = 0.0488, wR2 = 0.1121

These data can be obtained free of charge from The Cambridge Crystallographic Data Centre via www.ccdc.cam.ac.uk/data_request/cif.

3.2 Single-crystal Structure and Packing of 2

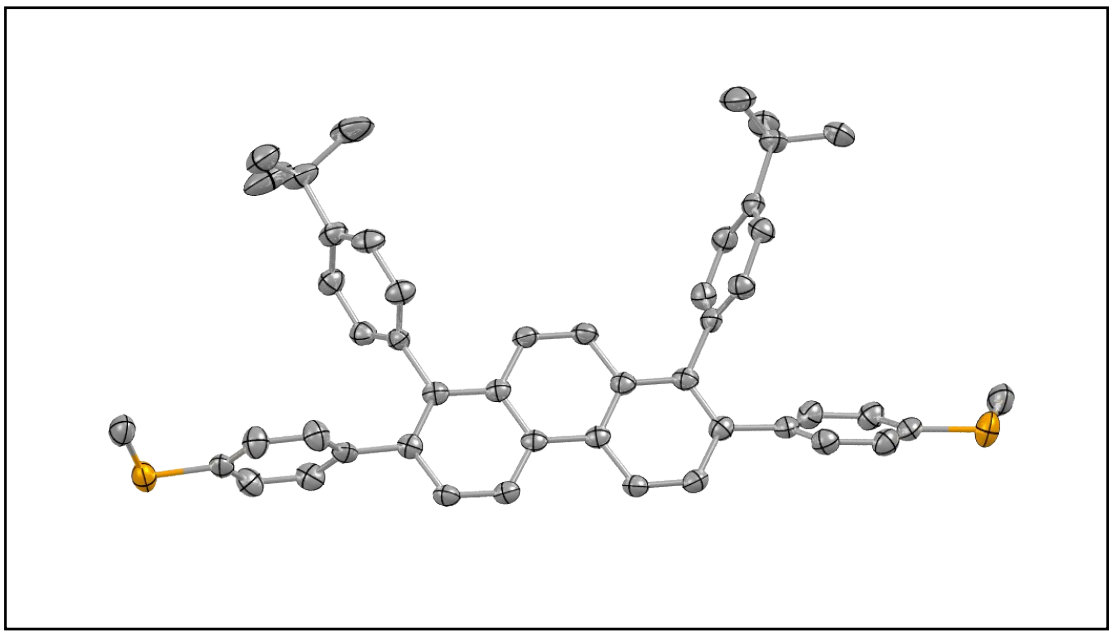

Figure S1. X-ray crystallographic structures of **2** (thermal ellipsoids shown at 75% probability, hydrogen atoms were omitted for clarity).

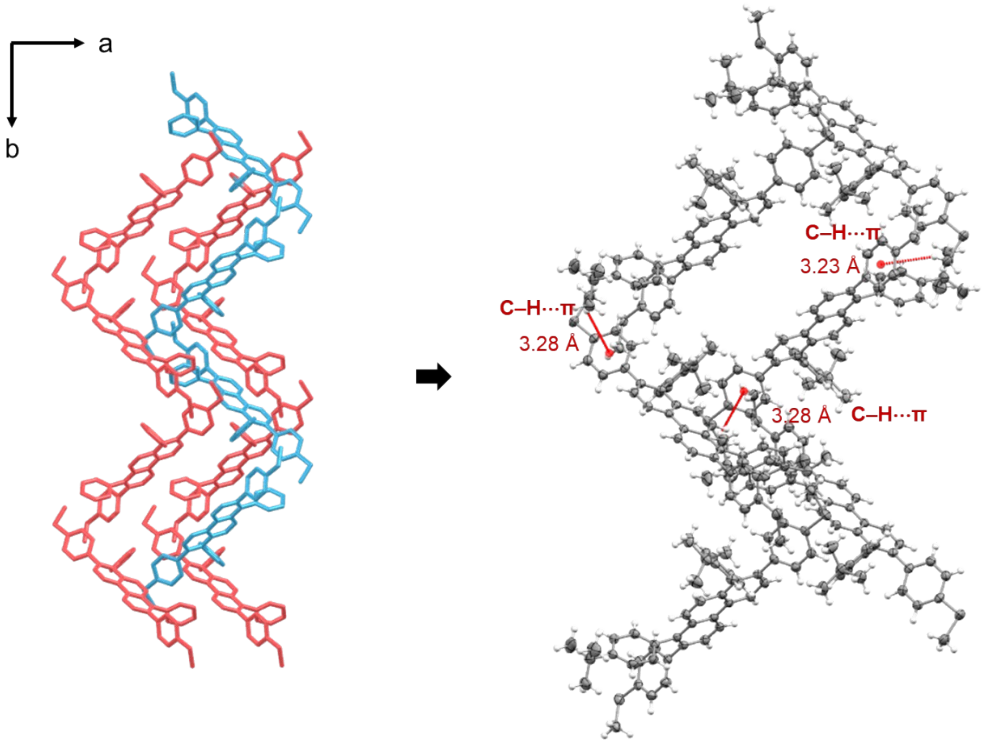

Figure S2.The packing structure of **2.**

4. The photophysical properties

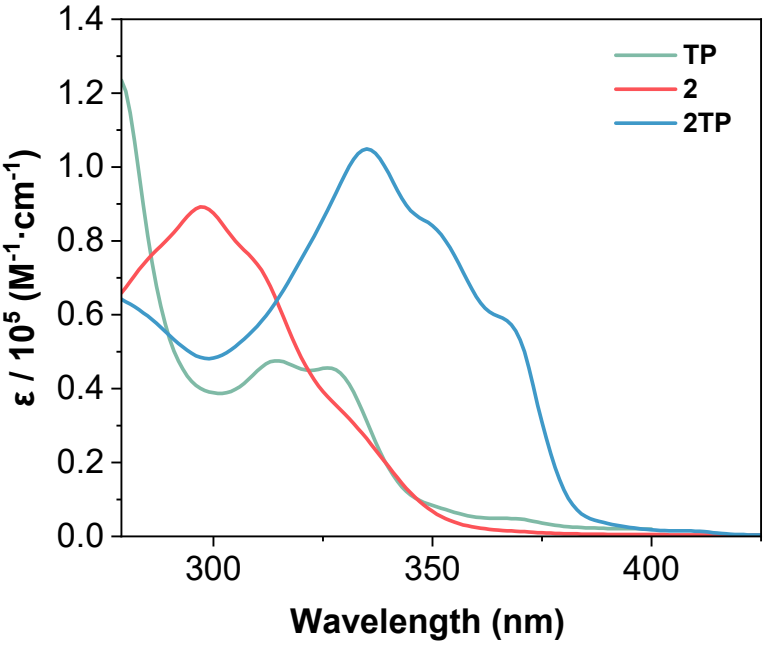

Figure S3. Absorption spectra of **TP**, **2** and **2TP** in DCM solutions. (1.0×10^{-5} mol/L in DCM).

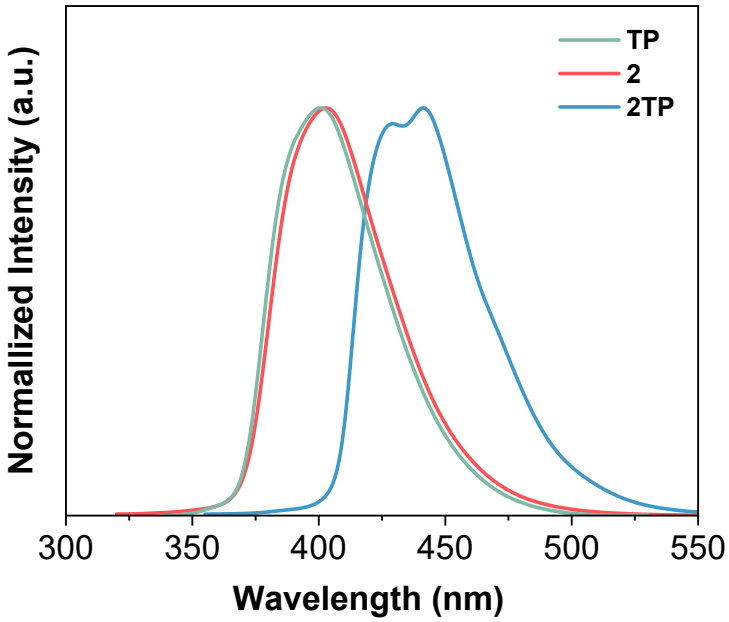

Figure S4. Liquid fluorescence emission spectra of **TP**, **2** and **2TP** in DCM solutions. (1.0×10^{-5} mol/L in DCM for liquid fluorescence emission spectra).

Table S2. Spectroscopic Characterizations of **TP**, **2** and **2TP**.

compound	λ_{abs} **[nm]**	ε_{max} **[10^5 M^{-1} cm^{-1}]**	λ_{em} **[nm]**	**Φ [%]**
TP	315	4.68	401	3
2	297	4.95	403	5
2TP	335	5.02	441	13

The absolute fluorescence quantum yields (Φ_F) are measured by using an integrating sphere detector.[3] In CH_2Cl_2 solution, Φ_F value increases with the ladderization of the backbone in **2** (5%) and **2TP** (13%), which is also attributed the enhancement of structural rigidity that suppresses the non-radiative transition.

5. Electrochemistry

Electrochemical measurements were performed at room temperature using a Metrohm Autolab PGSTAT204 potentiostat. Cyclic voltammetry (CV) and differential pulse voltammetry (DPV) were conducted in a conventional three-electrode system, comprising a glassy carbon working electrode (1.5 mm diameter), a platinum wire counter electrode, and an Ag/AgCl (3 mol L^{-1} KCl) reference electrode. The commercial supporting electrolyte salts, Na[BArF$_{24}$] and [^{n}Bu$_4$N][PF$_6$], were purified by recrystallization prior to use. [^{n}Bu$_4$N][BArF] was synthesized according to a literature procedure.[4] Measurements were carried out in dry DCM with analyte concentrations ranging from 0.1 to 1 mM.

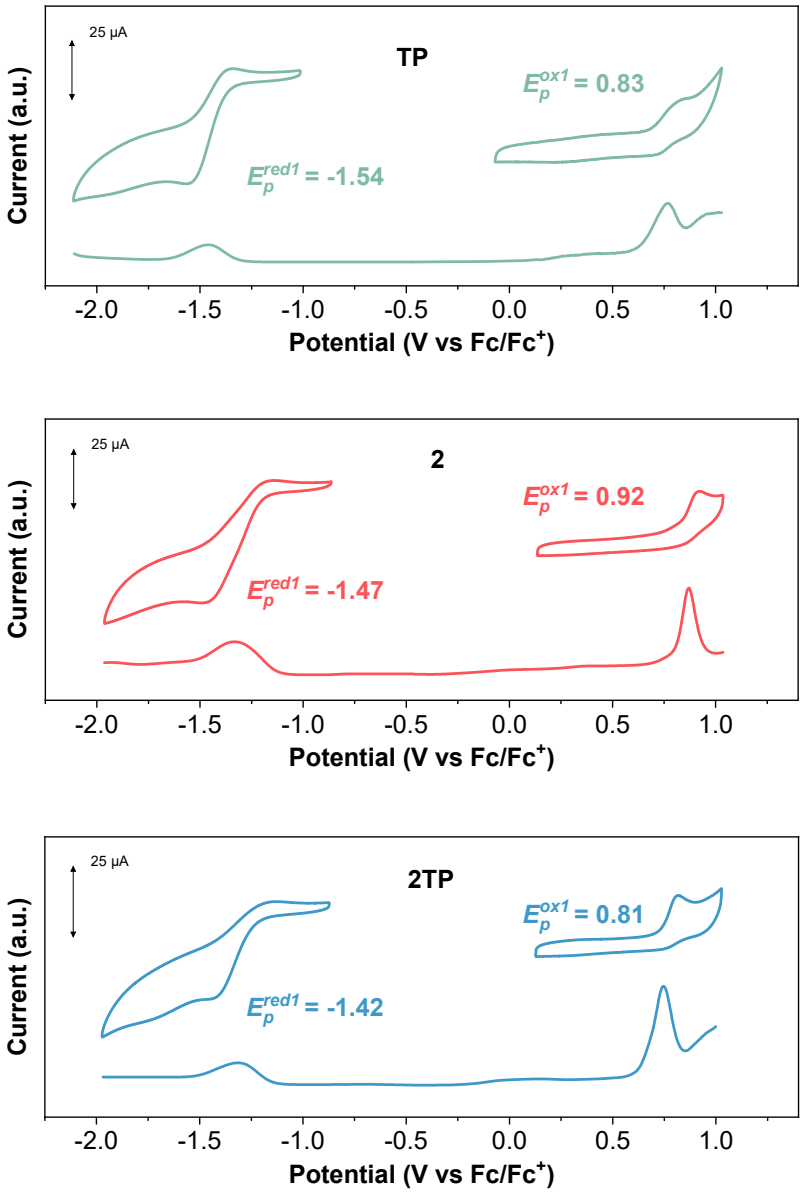

Figure S5. CV and DPV of **TP**, **2** and **2TP** (1.0×10^{-4} M) in DCM solutions containing

0.1 M Bu_4NPF_6 at a scan rate of 0.1 V/s and room temperature.

6. STM-BJ measurements

Single-molecule conductance measurements were performed at room temperature using the scanning tunneling microscope break-junction (STM-BJ) technique. The experiments were conducted in a solution of 1,2,4-trichlorobenzene (TCB, Sigma-Aldrich, ≥99.5%) containing 0.5 mM of the target molecule, with a constant bias voltage of 100 mV applied between the gold electrodes. The stretching rate of the gold electrodes was first calibrated following a previously established method[5] by repeatedly forming and breaking Au point contacts in pure TCB solvent as a control. The resulting 1D and 2D conductance histograms exhibited direct tunneling characteristics without clear plateaus, confirming a molecule-free gap in the control experiments. The relative displacement within the conductance range from 10^{-4} to 10^{-6} G_0 was calibrated using the measured tunneling decay constant ($\beta = -5.5\ nm^{-1}$). The calculated displacement over this range is $\Delta z = [\log(10^{-6}) - \log(10^{-4})] / \beta \approx 0.36$ nm.

Furthermore, the snap-back distance has also been calculated.[5] Because a perfect linear atomic chain of gold has a conductance of G_0, we assume that $\log(G/G_0) = -\alpha z$, where $z = 0$ corresponds to the point where the distance between the terminating gold atoms is equal to the equilibrium gold–gold separation. As the measured separation $\Delta z = z - z_{corr}$, where z_{corr} is the snap-back distance, a plot of $\log(G/G_0)$ versus Δz has a slope of $-\alpha$ and an intercept of $-\alpha z_{corr}$. The electrode stretching rate could be calibrated by measuring the conductance G versus Δz ranging from 10^{-4} to 10^{-6} G_0 to fit the slope and the intercept. From the repeated measurements, we obtained a displacement distribution of the intercepts extended from the range of 10^{-4} to 10^{-6} G_0 to a range of $10^{-0.3}$ to $10^{-6.0}$ G_0, in which the $10^{-0.3}$ G_0 is the zero–set point of the conductance–distance curve. The most probable displacement was found to be 0.5 nm, in agreement with our previous studies, which is the snap-back distance previously calibrated in the gold electrode system.

An automated control program was used to identify plateaus in the results by applying preset conductance ranges. We measured the solution containing the target molecule and calculated the conductance range of the target molecule. In the case that a selected threshold is reached in the conductance range, which means a stable molecular junction is formed, the piezoelectric movement is paused, keeping the molecular junction within such a conductance range of 100 ms. The measurement mode is then changed to the *I-V* measurement mode with a bias range of ±1.5 V. If the measured conductance is still within the predetermined range, the measured *I-V* curve is collected for subsequent statistical analysis.

The estimation of conductance suppression by the twisted conformation is conducted by the linear function that describes the relationship between conductance and the twisted angle (θ).[6] By transforming the function from absolute conductance value to the relative conductance suppression (%), the suppressed conductance ratio could be expressed as:

$$G_{percentage} = 97.58 \times \cos^2\theta + 1.58$$

The θ in planar **2TP** is set to 0, and the θ in twisted molecule **2** is obtained from the optimized structure as 53.4º. Thus, if the conductance of molecule **2** was controlled solely by the conformation, it should be about 0.9 orders lower than that of molecule **2TP**.

As the transition voltages of the molecular junction are asymmetric, the energy offset of the nearest conductive orbital was calculated as follow:[7, 8]

$$\varepsilon_h = 2\frac{e|V_+V_-|}{\sqrt{V_+^2 + \frac{10|V_+V_-|}{3} + V_-^2}}$$

Where V_+ is the transition voltage found in the positive range and V_- is the transition voltage found in the negative range.

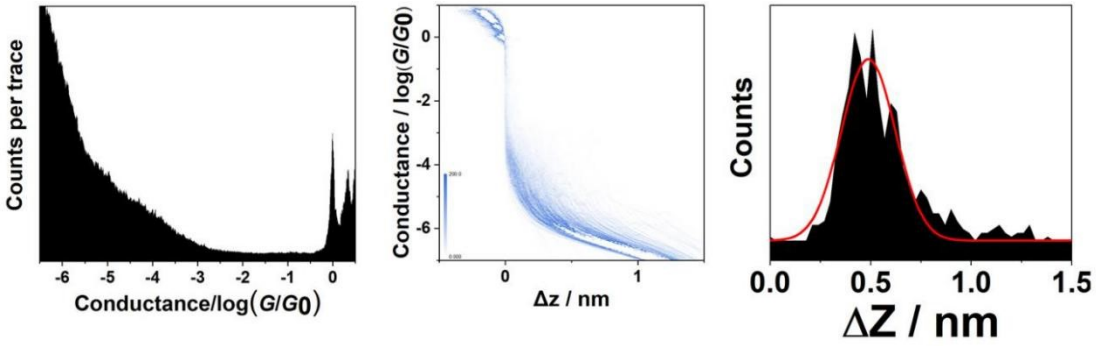

Figure S6. Histograms of pure solvent. From left to right, one-dimension conductance histogram, two-dimension conductance histogram and the relative displacement distribution determined from $10^{-0.3}$ G_0 to $10^{-6.0}$ G_0 for the calibration of the stretching rate of the electrodes pair.

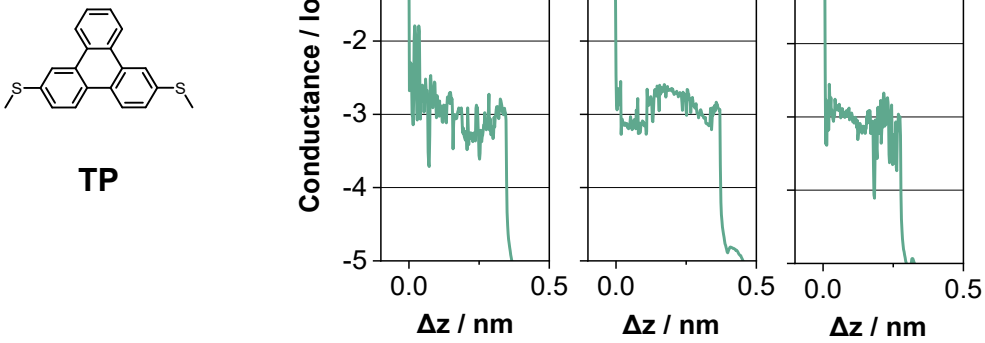

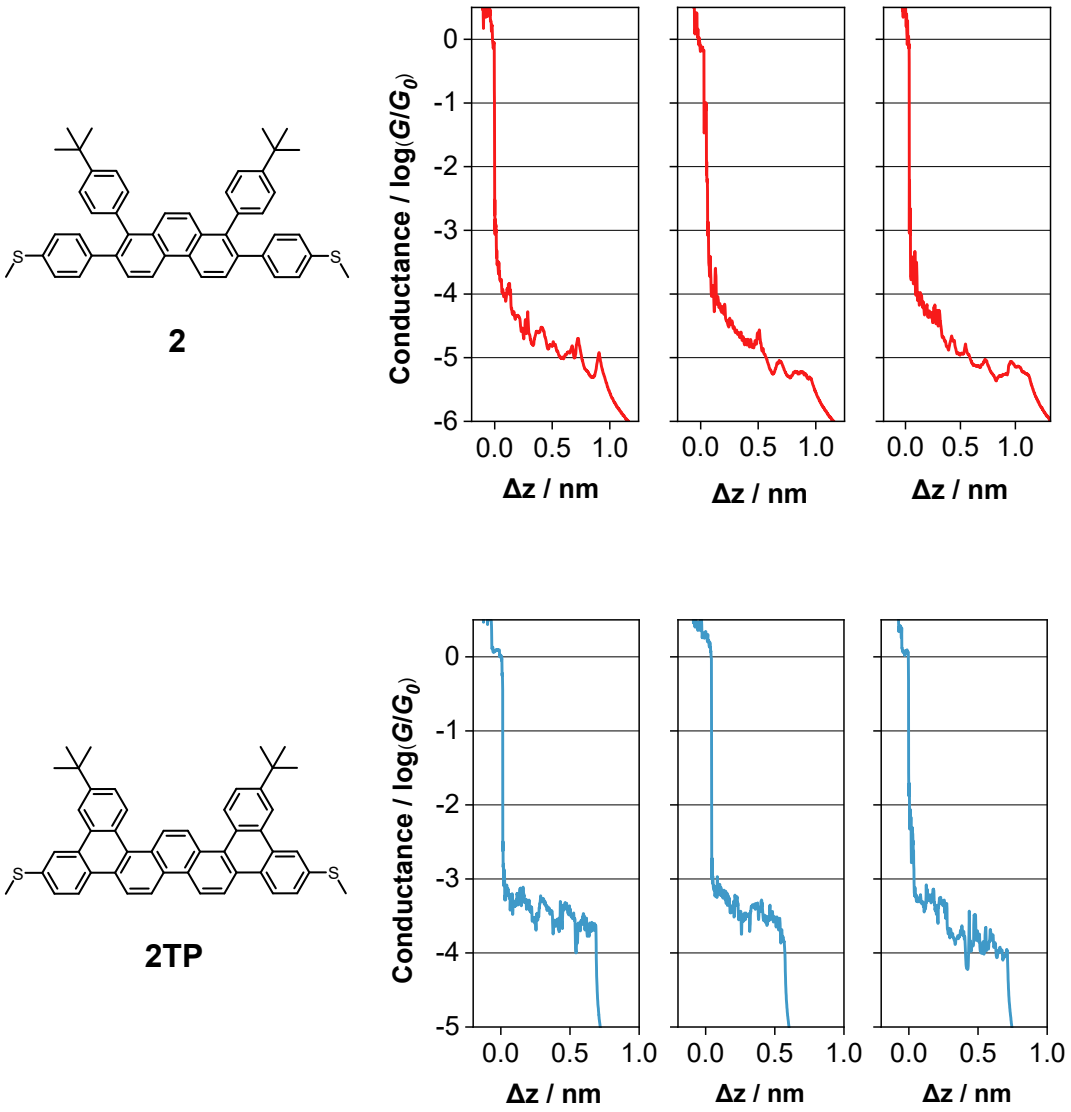

Figure S7. Typical conductance–displacement traces of **TP, 2** and **2TP.**

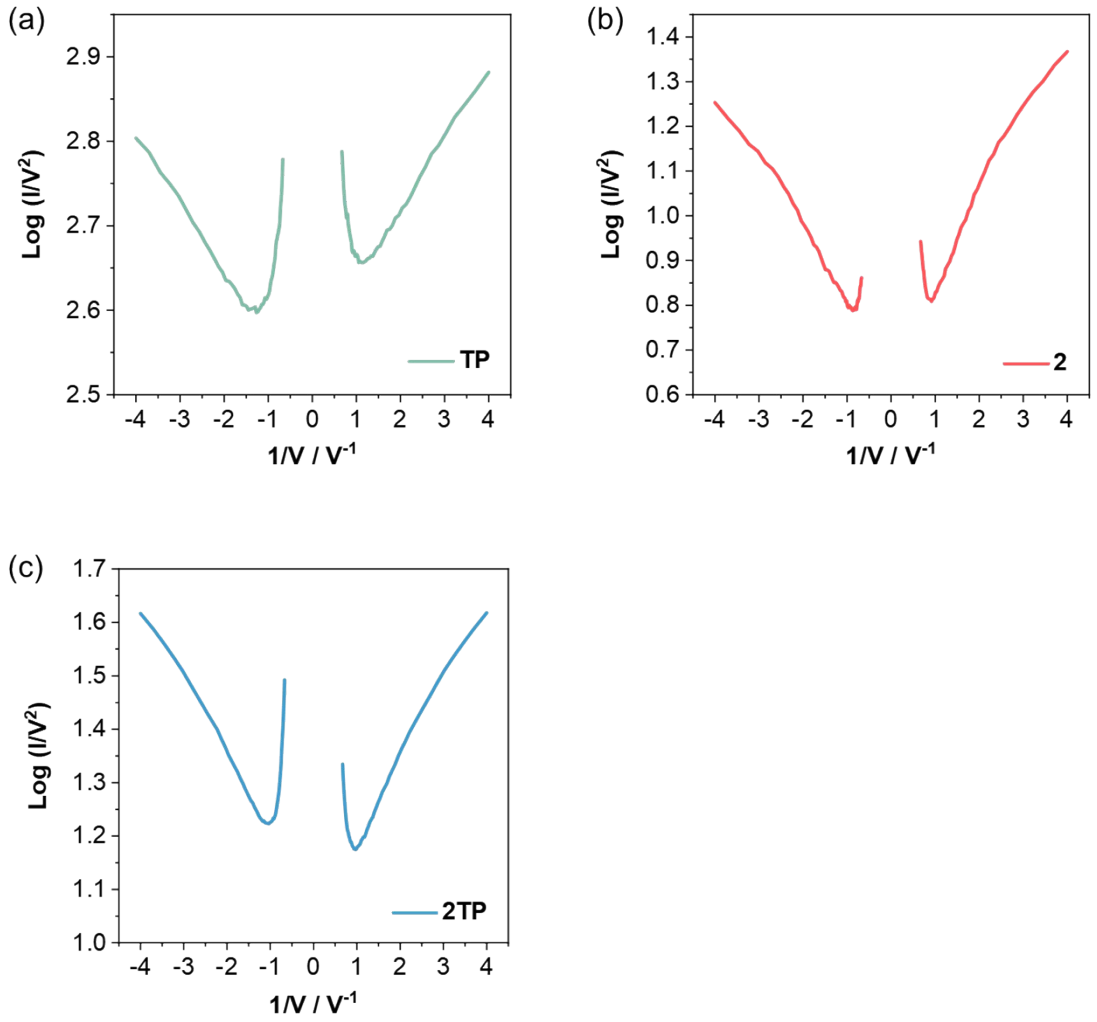

Figure S8. Fowler–Nordheim plots of **TP**, **2** and **2TP.**

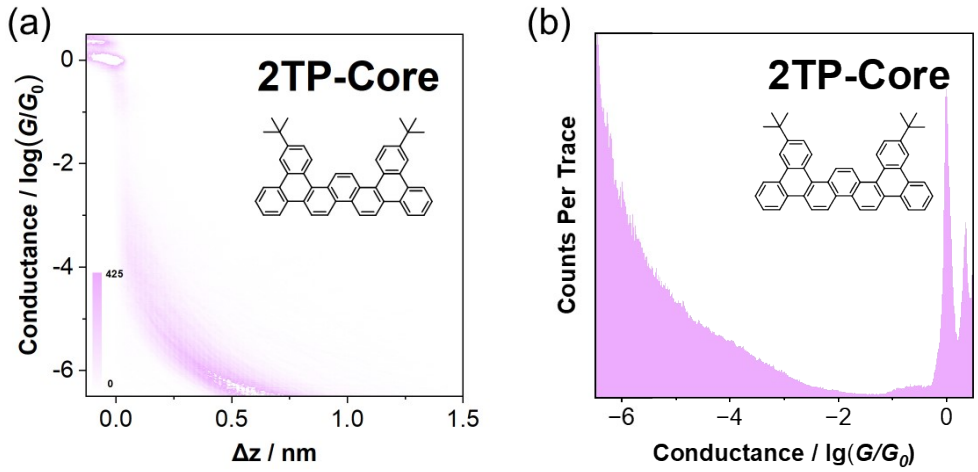

Figure S9. (a) 1D conductance histograms constructed from 2981 conductance – distance traces for **2TP-Core**. (b) 2D conductance distance histograms of **2TP-Core.**

Table S3. The transition voltage values of **TP**, **2** and **2TP**.

compound	the positive transition voltage	the negative transition voltage
TP	0.87 V	−0.81 V
2	1.10 V	−0.97 V
2TP	1.07 V	−0.93 V

7. Calculated details

All density functional theory (DFT) calculations were performed as follows. Ground-state geometry optimizations and frequency analyses were conducted using Gaussian 16 (Revision C.01)[9] at the 6-31G(d,p) level of theory.[10] The solvation effects of dichloromethane (DCM) were incorporated via the integral equation formalism variant of the Polarizable Continuum Model (IEF-PCM), with a standard state of 1 M.[11] Vibrational frequency analyses confirmed that optimized structures were either local minima (no imaginary frequencies) or first-order saddle points (one imaginary frequency) on the potential energy surface. These analyses also provided thermal corrections to obtain Gibbs free energies at 298.15 K. The intrinsic reaction coordinate (IRC) path was traced for each transition state to verify its connection to the correct reactants and products.

High-accuracy single-point electronic energies were computed on the optimized geometries using ORCA 5.0.4[12-15] at the RI-ωB97M-V/def2-TZVP level of theory, employing the def2/J auxiliary basis set.[16-19] The solvation model based on density (SMD) was applied with a standard state of 1 M.[20] To ensure accuracy, the geometrical counterpoise (gCP) correction[21] was applied to mitigate basis set superposition error (BSSE), and Grimme's quasiharmonic correction[22] was employed with the Shermo 2.4 program[23] to derive thermochemical properties at 298.15 K. Optimized molecular structures were visualized using VMD 1.9.3.[24]

To identify the most suitable functional for excited-state calculations, time-dependent DFT (TD-DFT) calculations were benchmarked against experimental data. These benchmarks were performed with Gaussian 16 using the 6-31G(d,p) basis set and IEF-PCM (DCM, 1 M standard state), testing a range of functionals: B3LYP-D3(BJ), PBE0-D3(BJ), PBE38, CAM-B3LYP, ωB97XD, and M06-2X.[25-29] The benchmarking results identified PBE0-D3(BJ) as the functional providing the closest agreement with experimental data, and it was therefore employed for all subsequent TD-DFT analyses.

To further elucidate the photophysical properties, the energy diagrams and frontier molecular orbitals of **TP**, **2** and **2TP** are calculated by the time-dependent density functional theory (TD-DFT) method (Figures S17–19).[30] The lowest energy absorption bands of **2** and **2TP** are attributed to the $S_0 \rightarrow S_3$ excitation, which mainly arises from the HOMO-1 → LUMO+1 transition and HOMO → LUMO+1 transition respectively. The results also show an oscillator strength (f) of 0.95 for **2** and 1.28 for **2TP**. Moreover, the lowest energy absorption bands of **TP** is attributed to the $S_0 \rightarrow S_6$ excitation arisen from the HOMO-1 → LUMO+1 transition and displayed a oscillator strength (f) of 0.32.

The molecular structures were optimized using the B3LYP/6-31G* level6 of theory in the Gaussian16 package.[9] Following potential energy surface scanning with generalized internal coordinates (GIC), two distinct stable conformations were

identified and further optimized.

The charge transport properties of these molecular junctions were calculated after geometry optimization within the density functional theory (DFT) framework, employing the combined DFT and non-equilibrium Green's function (NEGF) formalism. These calculations were conducted using the Quantum Atomistix ToolKit (ATK, Q-2019.12 version).[31] During device modelling, the two gold (111) electrodes consist of a unit cell 13×10 and the extension region thickness is seven gold layers to guarantee rational molecular device modelling. A pyramid-shaped gold cluster with six layers was employed to form the stable contact with the target molecules. In the NEGF-DFT calculations, we adopted the exchange-correlation Generalized Gradient Approximation (GGA) with the Perdew-Burke-Ernzerh (PBE) parameterization for molecular device calculations. we used FHI pseudopotentials and a double-ζ polarized (DZP) atomic orbital basis set (except for double-ζ for gold atom). Exchange-correlation effects were handled at the Perdew-Burke-Ernzerh (PBE) exchange-correlation generalized gradient approximation (GGA) level. The real-space grid used a 150 Hartree cut-off, with a default 4×4×150 k-point grid in the calculation of the transmission spectrum. The optimization of geometry and adsorption in ionic liquids at zero bias was optimized using the convergence criterion of 0.02 eV/A. Transmission spectra calculation was conducted with sampling of 7×7 k-points.

7.1 Calculated molecular geometries

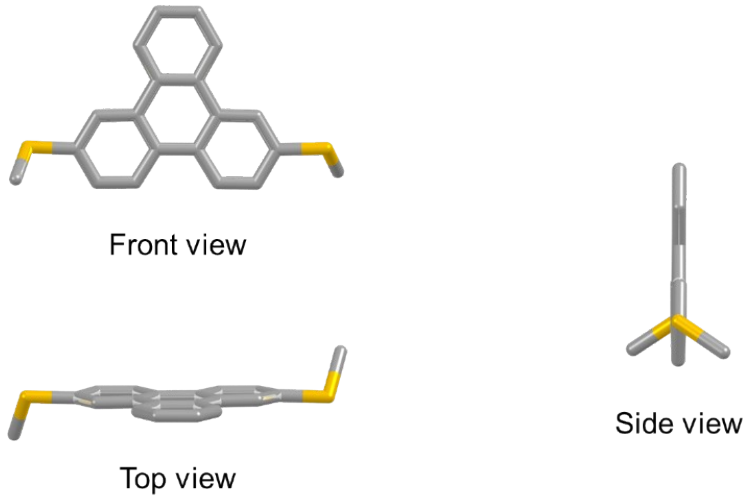

Figure S10. Molecular geometry of **TP** optimized by DFT calculation.

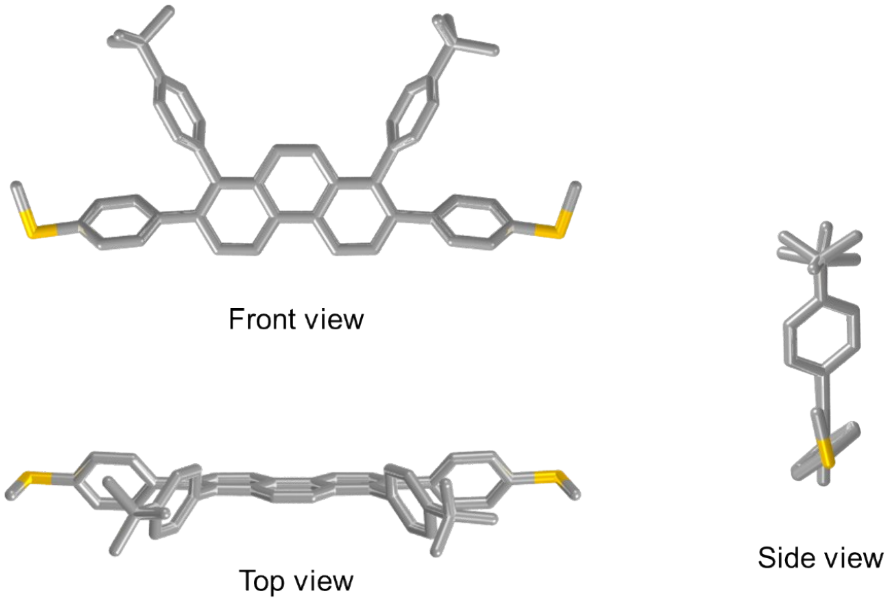

Figure S11. Molecular geometry of **2** optimized by DFT calculation.

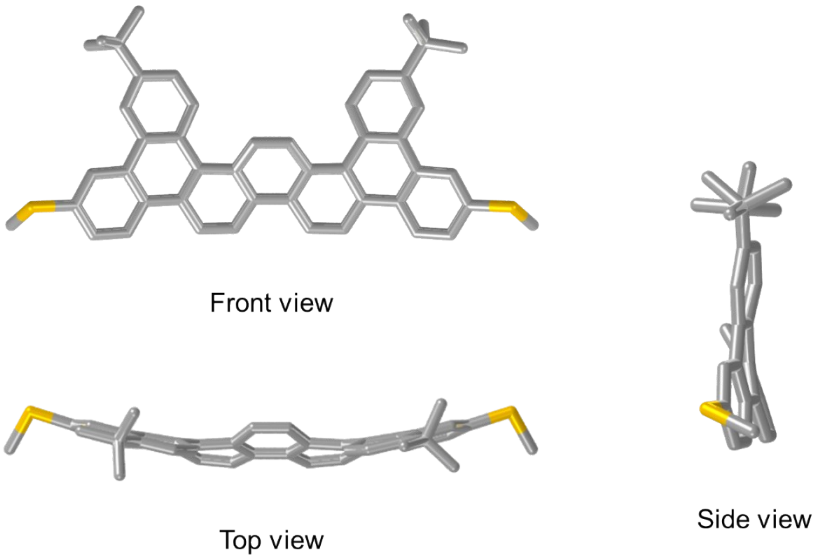

Figure S12. Molecular geometry of **2TP** optimized by DFT calculation.

7.2 Frontier molecular orbitals

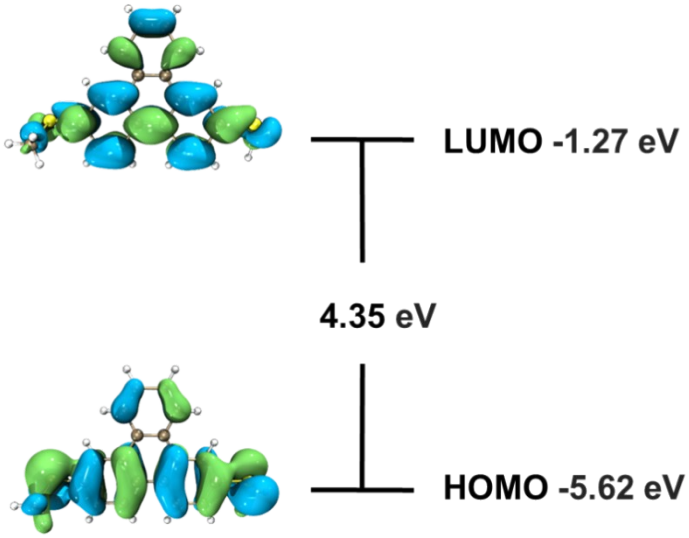

Figure S13. The frontier molecular orbitals of **TP** calculated at the B3LYP/6-31G(d) level of theory.

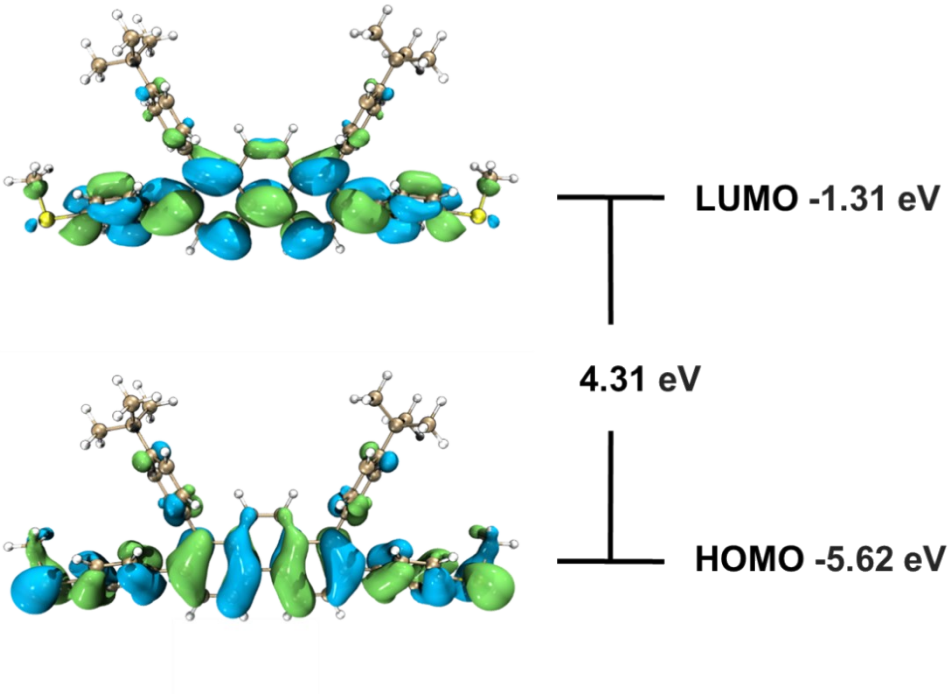

Figure S14. The frontier molecular orbitals of **2** calculated at the B3LYP/6-31G(d) level of theory.

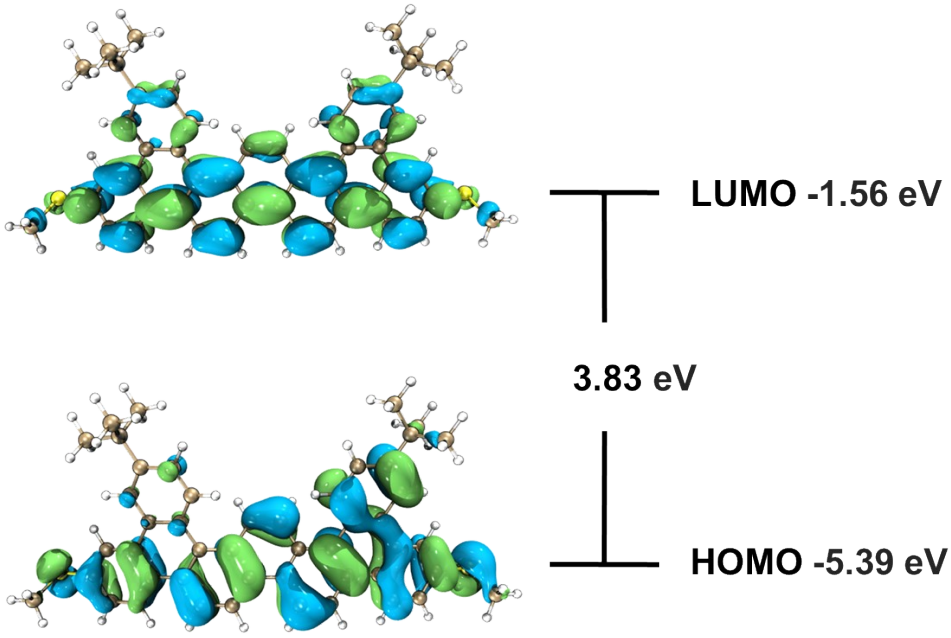

Figure S15. The frontier molecular orbitals of **2TP** calculated at the B3LYP/6-31G(d) level of theory.

7.3 Electronic structures and molecular aromaticity

Table S4. The aromaticity values of **TP** by density functional theory (DFT) calculations based on B3LYP/6-31G(d)

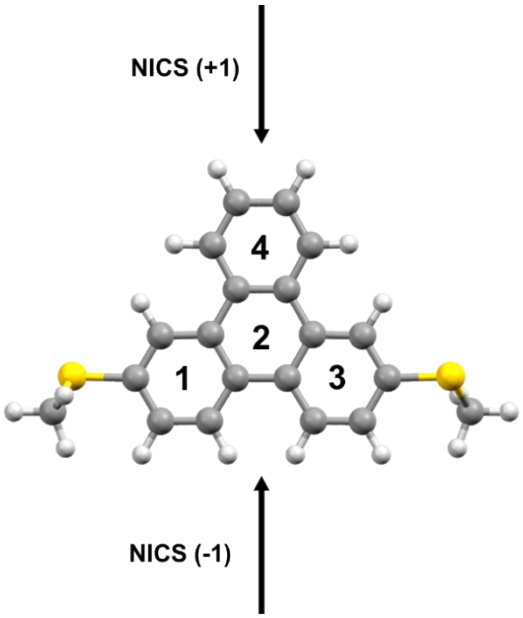

Ring	NICS(0)	NICS(+1)	NICS(-1)	$NICS(+1)_{zz}$
1	-8.61	-10.46	-10.46	-23.84
2	-2.91	-6.17	-6.17	-9.92
3	-8.61	-10.46	-10.46	-24.25
4	-9.07	-10.97	-10.97	-26.35

Table S5. The aromaticity values of **2** by density functional theory (DFT) calculations based on B3LYP/6-31G(d)

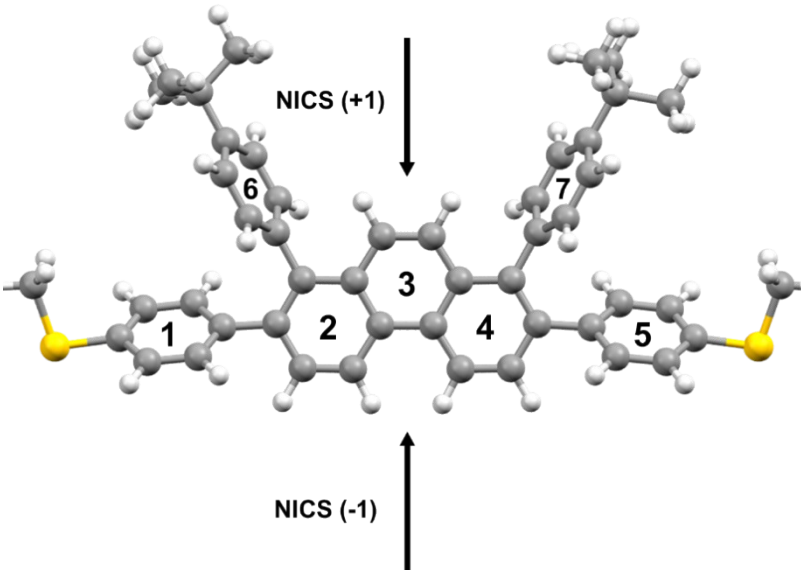

Ring	NICS(0)	NICS(+1)	NICS(-1)	$NICS(+1)_{zz}$
1	-9.03	-10.54	-10.48	-26.49
2	-8.88	-10.55	-10.48	-25.90
3	-6.23	-8.29	-9.22	-17.91
4	-8.88	-10.55	-10.48	-25.90
5	-9.02	-10.52	-10.48	-26.44
6	-8.63	-10.47	-10.22	-28.37
7	-8.63	-10.47	-10.22	-28.40

Table S6. The aromaticity values of **2TP** by density functional theory (DFT) calculations based on B3LYP/6-31G(d).

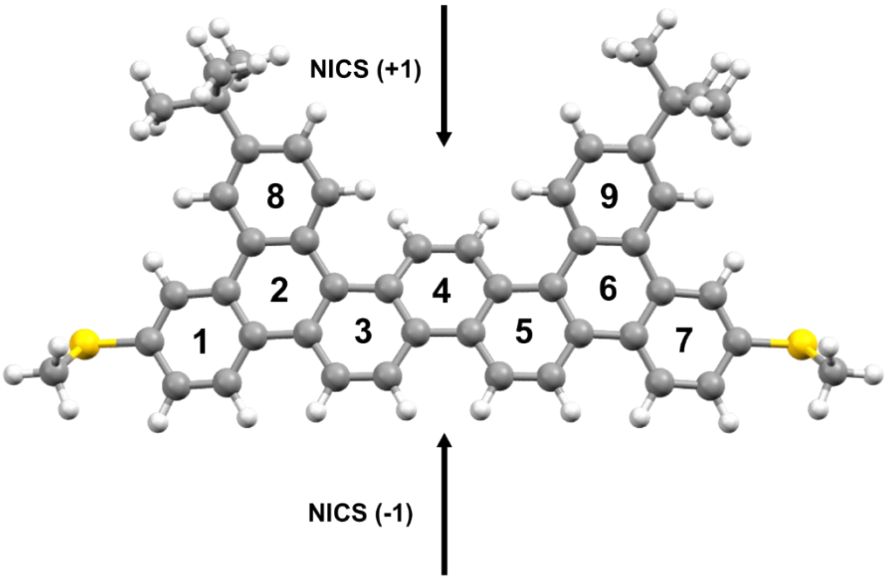

Ring	NICS(0)	NICS(+1)	NICS(-1)	$NICS(+1)_{ZZ}$
1	-8.59	-10.12	-10.73	-22.79
2	-2.84	-6.59	-5.96	-10.63
3	-7.60	-9.78	-10.17	-22.12
4	-6.79	-7.25	-11.12	-15.35
5	-7.59	-9.79	-10.15	-22.14
6	-2.52	-6.30	-5.69	-9.79
7	-8.52	-10.06	-10.67	-22.62
8	-8.89	-11.83	-9.80	-26.67
9	-9.16	-12.03	-10.03	-27.31

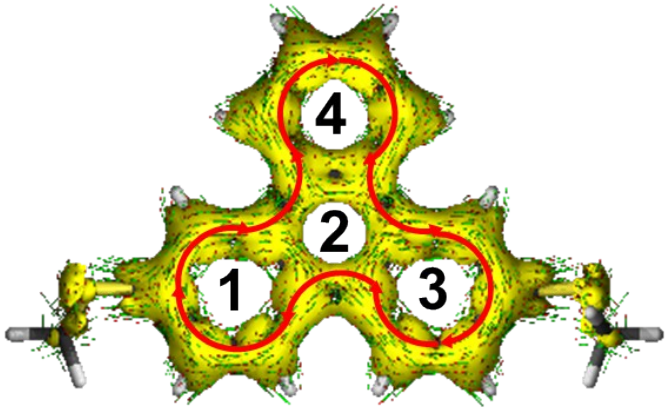

Figure S16. Anisotropy of the induced current densities (ACID) of **TP** by density functional theory (DFT) calculations based on B3LYP/6-31G(d).

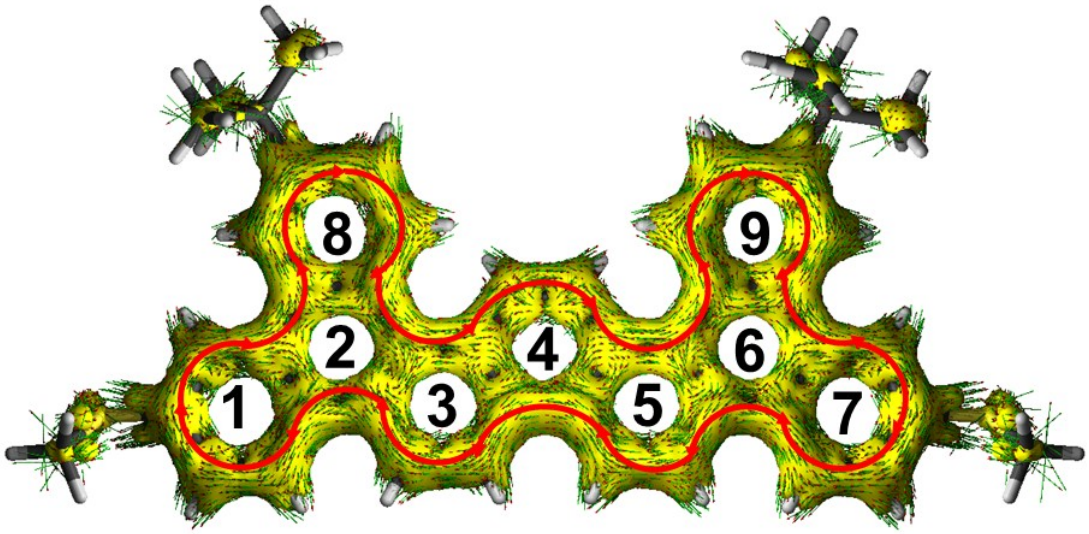

Figure S17. Anisotropy of the induced current densities (ACID) of **2TP** by density functional theory (DFT) calculations based on B3LYP/6-31G(d).

7.4 TD-DFT calculation

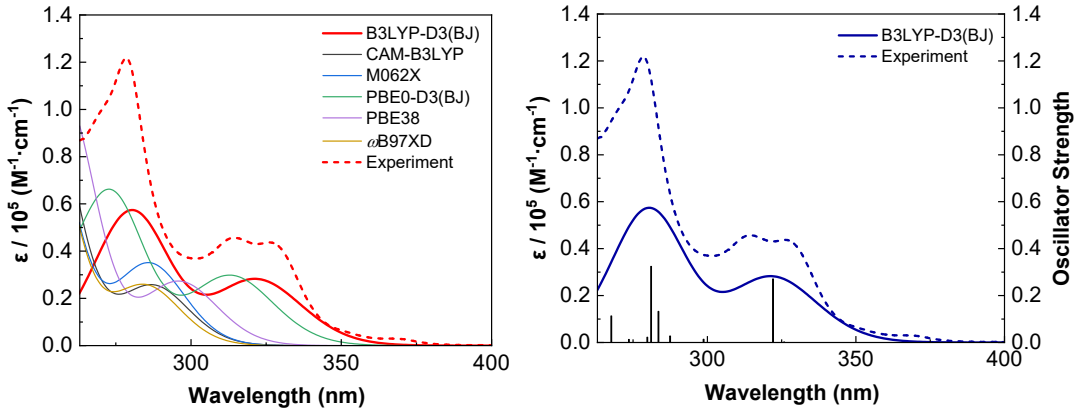

Table S7. Major electronic transitions for **TP** by TD-DFT method using B3LYP-D3(BJ)/6-31G(d,p).

Transition	Energy (eV)	Wavelength (nm)	Osc. Strength	Major contributions
S1	3.8050	325.85	0.0021	H-1 > L: 34.1%; H > L+1: 63.6%;
S2	3.8492	322.10	0.2708	H-1 > L+1: 7.7%; H > L: 90.9%;
S3	4.1504	298.73	0.0139	H-3 > L: 10.1%; H > L+2: 81.2%;
S4	4.3131	287.46	0.0279	H-2 > L: 91.9%;
S5	4.3728	283.54	0.1328	H-3 > L+1: 19.0%; H-1 > L: 42.3%; H-1 > L+2: 5.0%; H > L+1: 27.0%;
S6	4.4110	281.08	0.3245	H-4 > L: 5.4%; H-3 > L: 29.1%; H-1 > L+1: 54.2%;
S7	4.4314	279.78	0.0225	H-3 > L+1: 19.2%; H-1 > L: 11.6%; H-1 > L+2: 58.3%;
S8	4.5314	273.61	0.0131	H-2 > L+1: 89.2%;
S9	4.6318	267.68	0.1134	H-3 > L: 55.0%; H-1 > L+1: 27.9%; H > L+2: 6.1%;
S10	4.7648	260.21	0.0237	H-4 > L+1: 6.4%; H-2 > L+2: 84.3%;

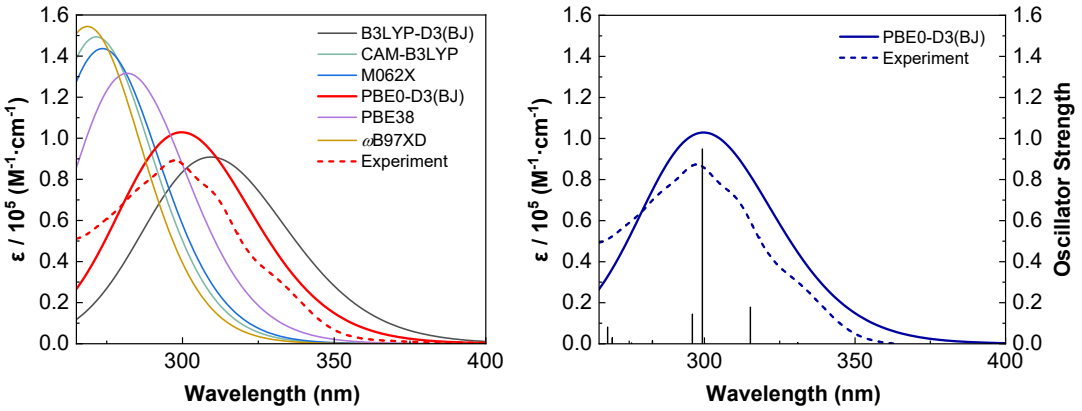

Table S8. Major electronic transitions for **2** by TD-DFT method using PBE0-D3(BJ)/6-31G(d,p).

Transition	Energy (eV)	Wavelength (nm)	Osc. Strength	Major contributions
S1	3.7453	331.04	0.0053	H-1 > L: 62.7%; H > L+1: 26.5%;
S2	3.9329	315.25	0.1789	H-1 > L+1: 20.9%; H > L: 74.5%;
S3	4.1423	299.31	0.9493	H-1 > L+1: 70.1%; H > L: 19.2%;
S4	4.1891	295.97	0.1450	H-2 > L: 16.0%; H-1 > L: 26.5%; H > L+1: 46.8%;
S5	4.3854	282.72	0.0151	H-3 > L+2: 5.4%; H-2 > L: 67.6%; H > L+1: 15.5%;
S6	4.4954	275.80	0.0047	H-3 > L: 50.5%; H-2 > L+1: 28.8%; H-2 > L+2: 5.9%;
S7	4.6029	269.36	0.0295	H-4 > L+1: 9.5%; H-3 > L: 25.6%; H-2 > L+1: 44.1%;
S8	4.6290	267.85	0.0818	H-5 > L: 45.9%; H-4 > L: 5.8%; H-1 > L+2: 34.3%;
S9	4.6879	264.48	0.0020	H-5 > L: 5.2%; H-4 > L: 66.6%; H-3 > L+1: 9.9%;
S10	4.7652	260.19	0.0102	H > L+2: 80.7%;

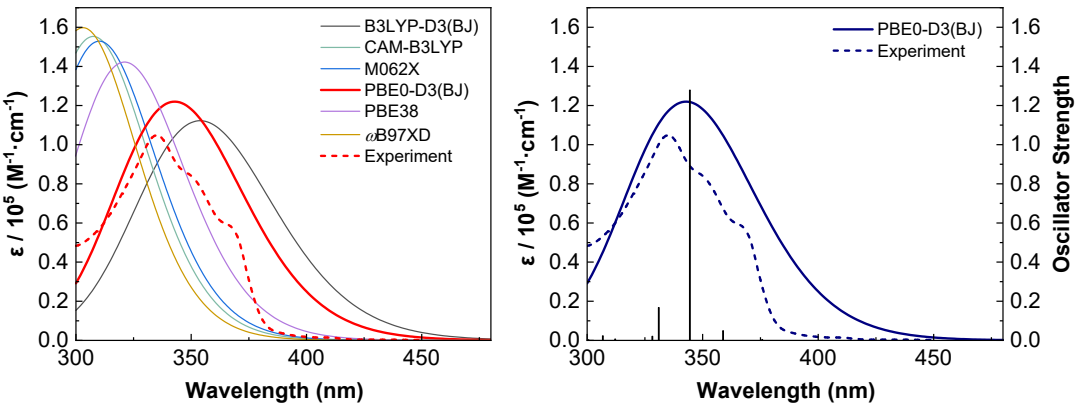

Table S9. Major electronic transitions for **2TP** by TD-DFT method using PBE0-D3(BJ)/6-31G(d,p).

Transition	Energy (eV)	Wavelength (nm)	Osc. Strength	Major contributions
S1	3.2993	375.79	0.0049	H-1 > L: 6.9%; H-1 > L+1: 24.7%; H > L: 58.5%;
S2	3.4551	358.84	0.0497	H-1 > L: 52.0%; H > L: 7.5%; H > L+1: 33.9%;
S3	3.5993	344.47	1.2790	H-1 > L: 33.7%; H-1 > L+1: 5.2%; H > L+1: 54.8%;
S4	3.7458	330.99	0.1679	H-2 > L: 10.1%; H-1 > L+1: 47.8%; H > L: 22.6%;
S5	3.7776	328.21	0.0210	H-3 > L: 35.7%; H-2 > L+1: 12.4%; H-1 > L+2: 26.8%; H > L+3: 13.5%;
S6	3.9721	312.14	0.0073	H-4 > L: 11.1%; H-3 > L+1: 8.9%; H-2 > L: 8.9%; H-1 > L+1: 5.2%; H-1 > L+3: 12.6%; H-1 > L+4: 6.3%; H > L+2: 24.8%;
S7	4.0412	306.80	0.0238	H-3 > L+1: 14.1%; H-2 > L: 34.3%; H-1 > L+1: 10.0%; H-1 > L+3: 15.8%; H > L+2: 6.7%;
S8	4.1244	300.61	0.0023	H-2 > L: 24.8%; H-1 > L+3: 7.7%; H > L+2: 40.5%;
S9	4.1861	296.18	0.0203	H-3 > L: 32.5%; H-1 > L+3: 7.7%; H > L+3: 38.3%;
S10	4.2200	293.80	0.0298	H-5 > L: 9.0%; H-2 > L+1: 51.4%; H-1 -> L+2: 11.6%; H-1 > L+5: 8.0%;

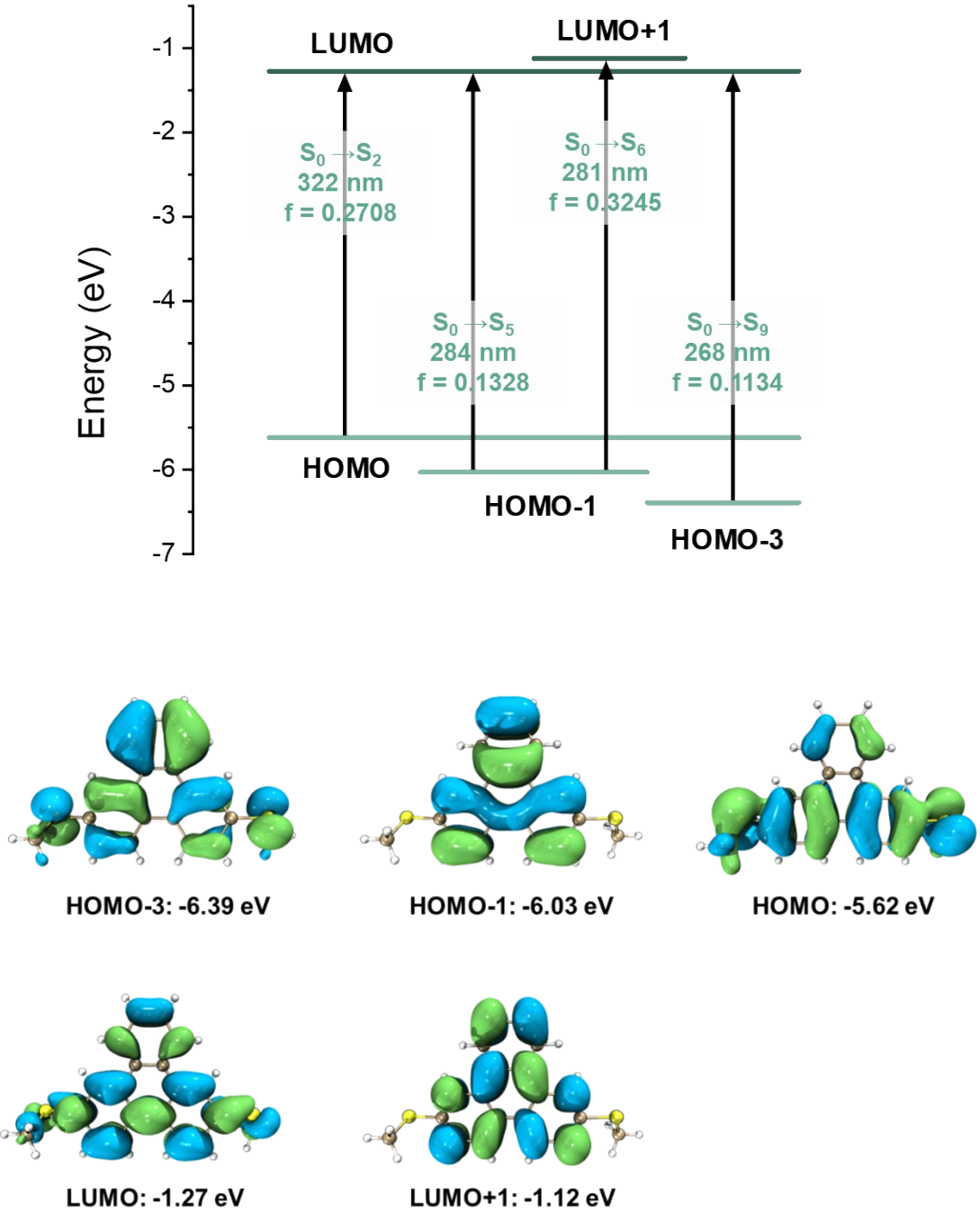

Figure S18. Energy diagrams and frontier molecular orbitals of **TP** calculated at the B3LYP-D3 (BJ)/6-31G(d,p) level of theory.

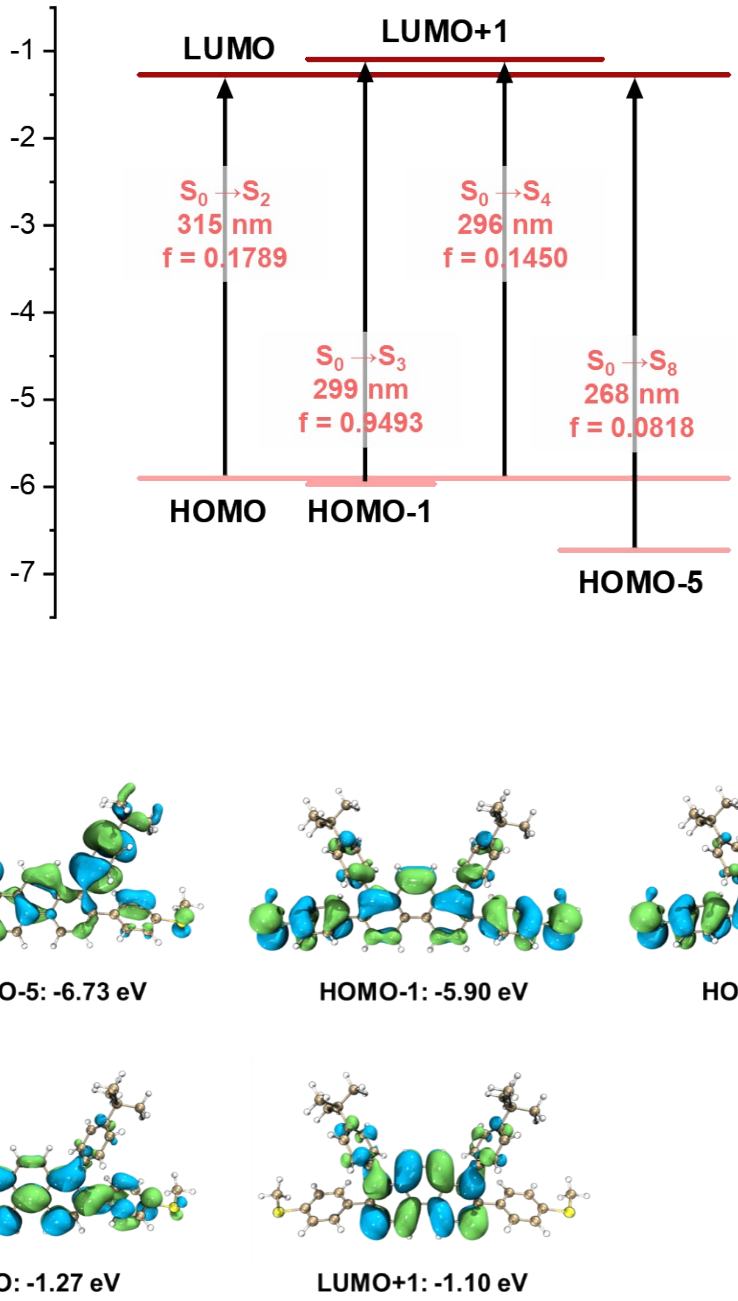

Figure S19. Energy diagrams and frontier molecular orbitals of **2** calculated at the PBE0-D3 (BJ)/6-31G(d,p) level of theory.

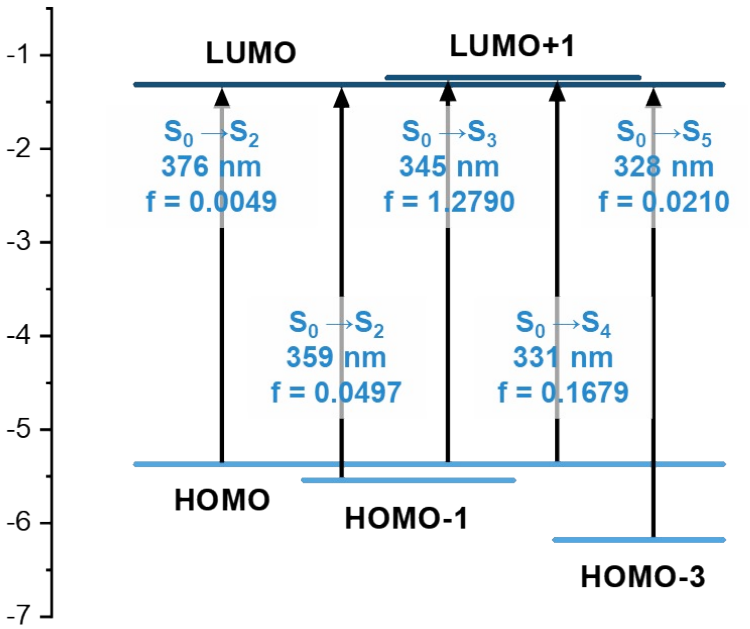

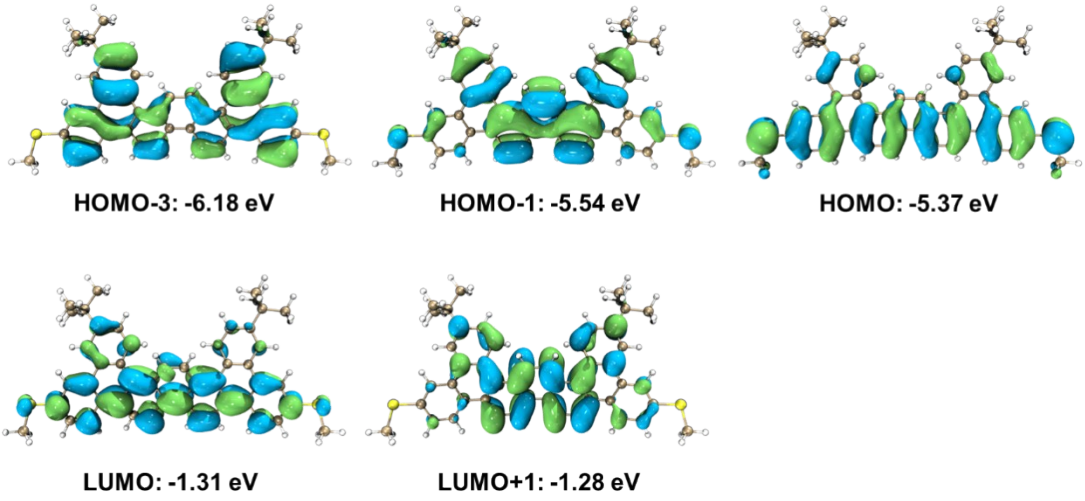

Figure S20. Energy diagrams and frontier molecular orbitals of **2TP** calculated at the PBE0-D3 (BJ)/6-31G(d,p) level of theory.

7.5 Theoretical calculations of transport properties

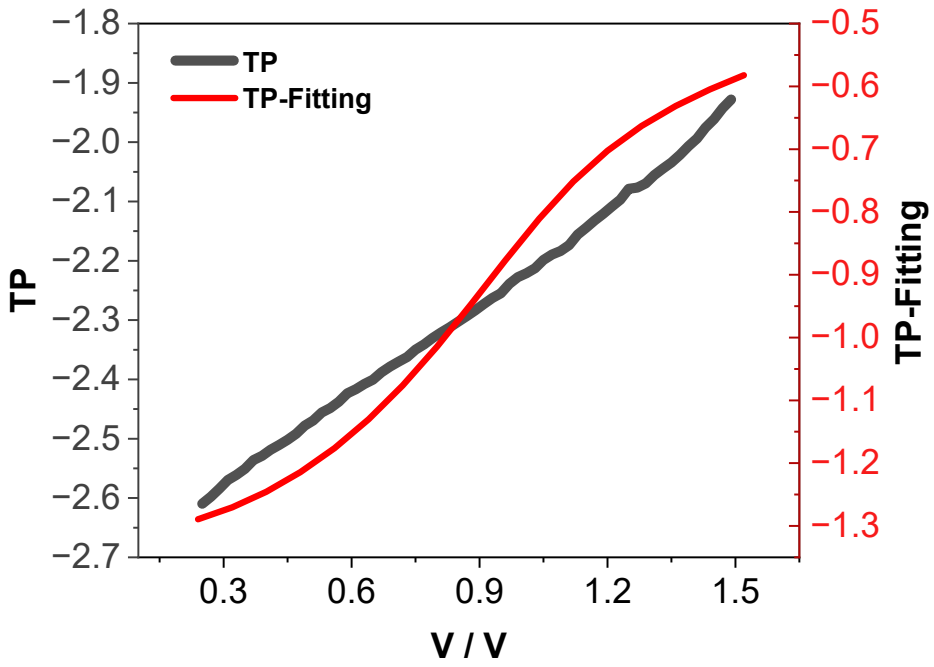

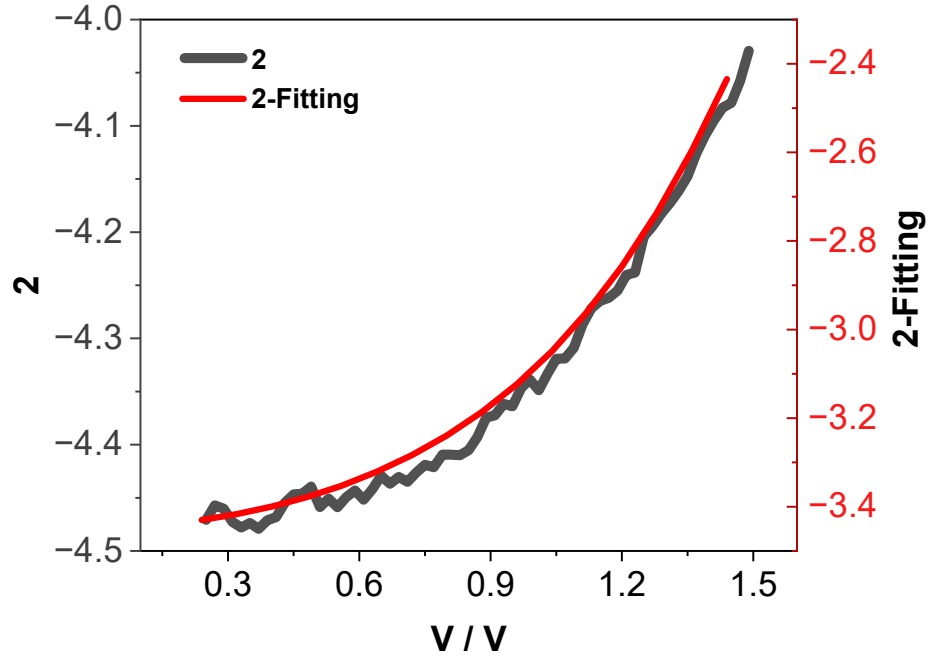

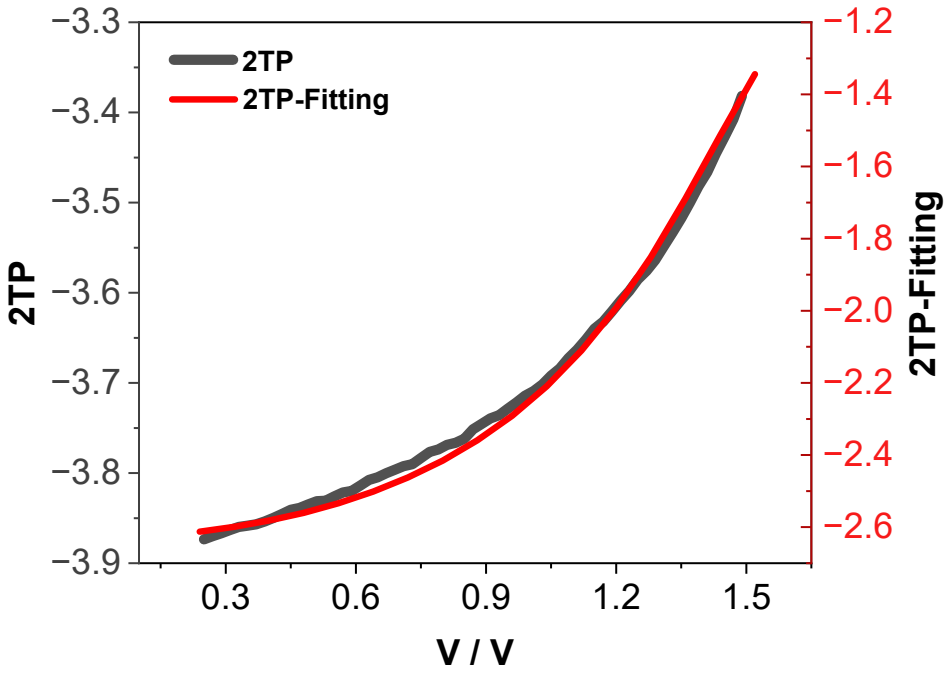

Figure S21. Fowler–Nordheim plots and Fitting plots of **TP**, **2** and **2TP.**

Table S10. The calculated orbital levels of **TP**, **2** and **2TP** junctions.

	TP	**2**	**2TP**
LUMO	1.37 eV	1.24 eV	1.23 eV
HOMO	**-1.67 eV**	**-1.72 eV**	**-1.43 eV**
E_F	-0.95 eV	-0.73 eV	-0.56 eV
$\Delta E_{LUMO-HOMO}$	3.04 eV	2.96 eV	2.66 eV
ε_h	0.72 eV	0.99 eV	0.87 eV

Table S11. Molecular projected self-consistent Hamiltonian (MPSH) and HOMO-1, HOMO, LUMO LUMO+1 and DOS (E_F) of **TP**, **2**, and **2TP** from devices calculated by Quantum ATK. Isoval = 0.02 e/Å^3.

	DOS (E_F)	LUMO+1	LUMO	HOMO	HOMO-1
TP	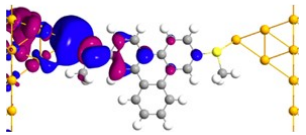	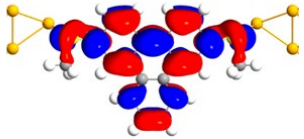	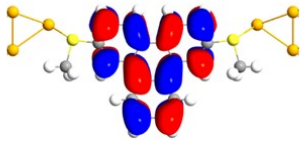	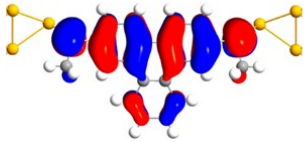	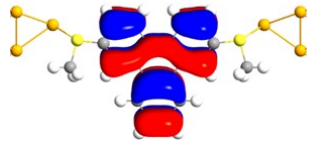
2	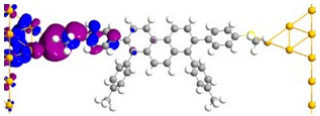	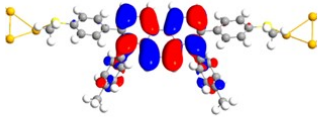	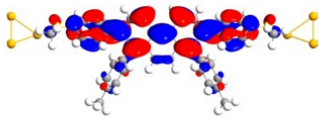	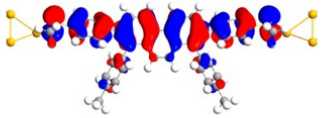	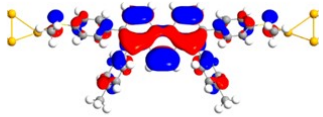
2TP	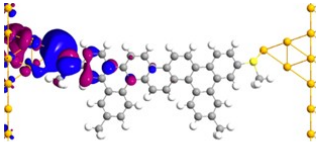	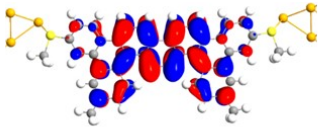	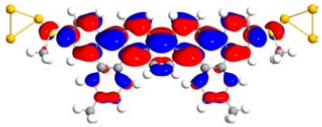	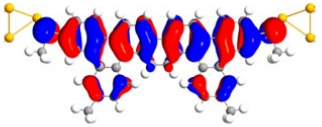	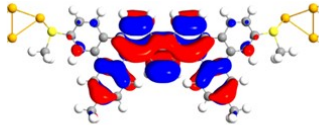

8. NMR spectra

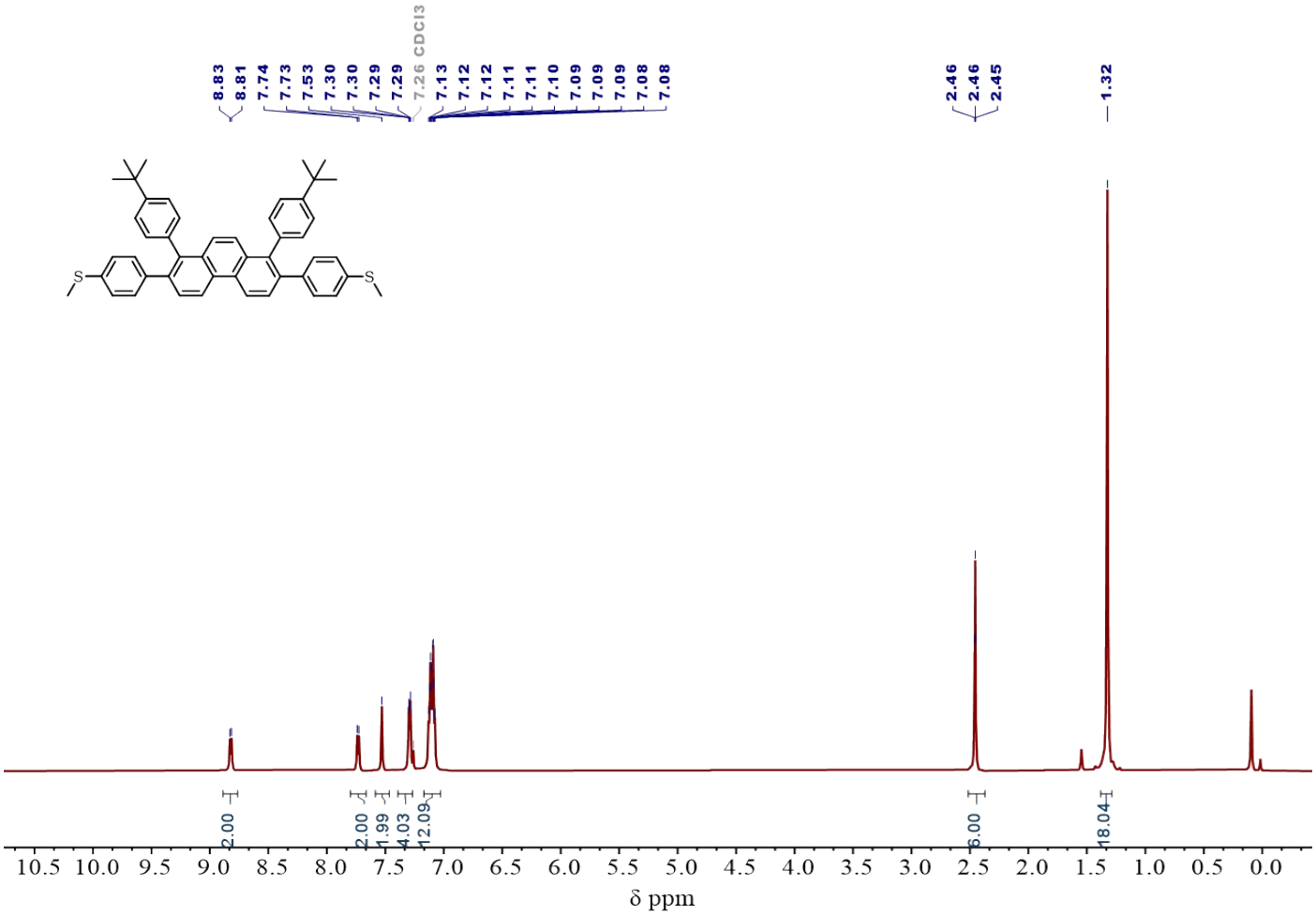

Figure S22. ^{1}H NMR spectrum (600 MHz, Chloroform-d) of **2.**

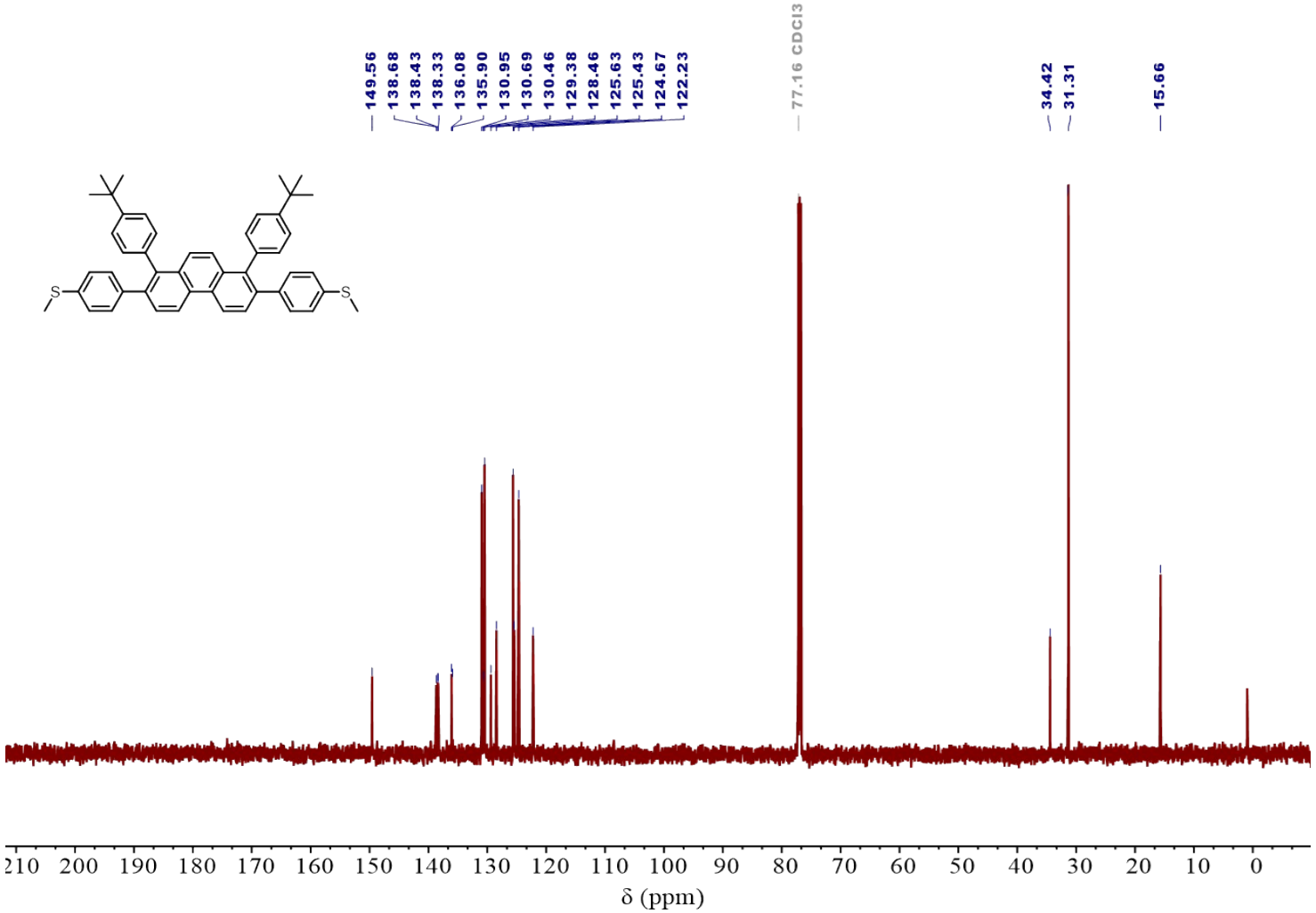

Figure S23. ^{13}C NMR spectrum (151 MHz, Chloroform-d) of **2**.

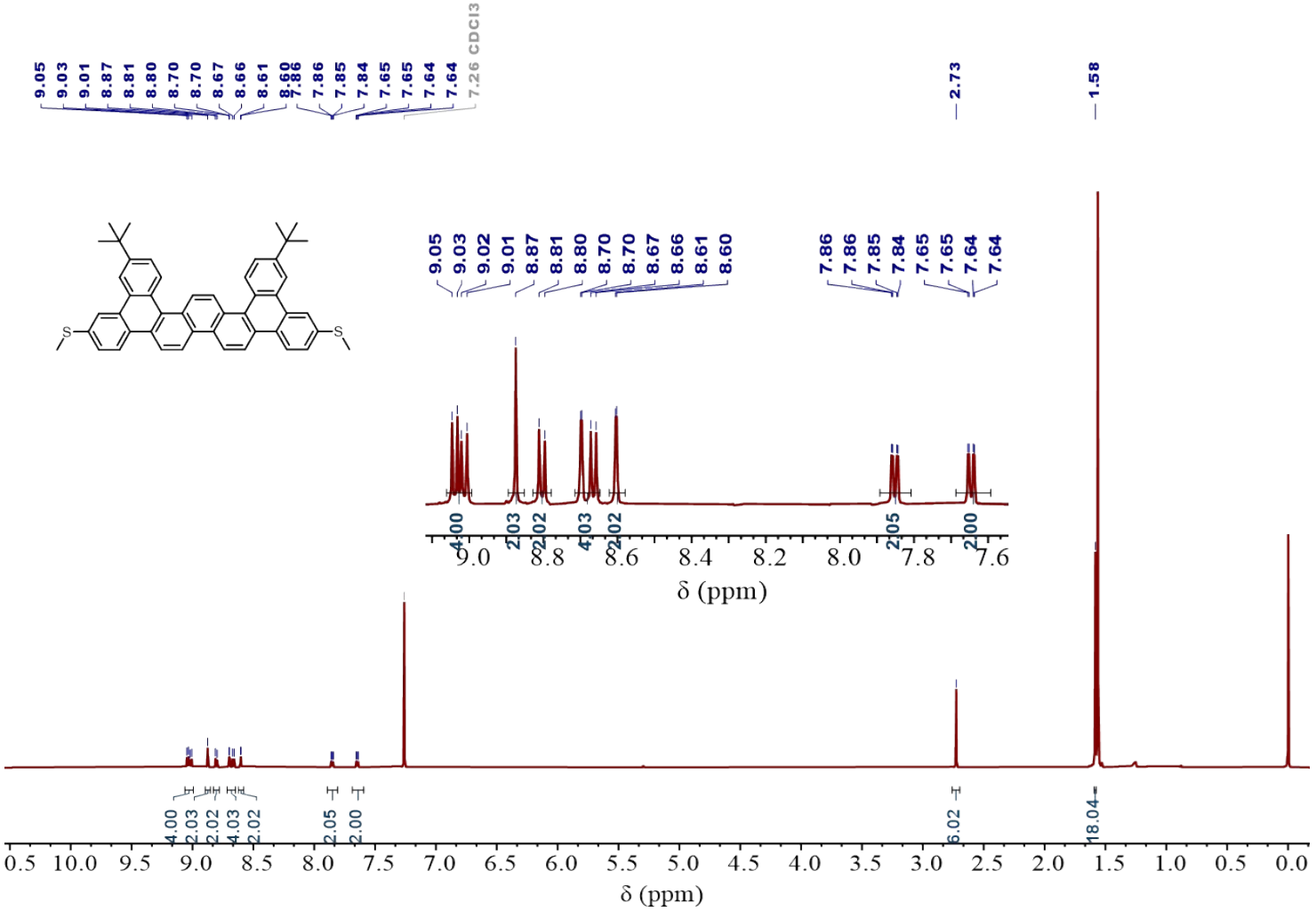

Figure S24. ^{1}H NMR spectrum(151 MHz, Chloroform-d) of **2TP**.

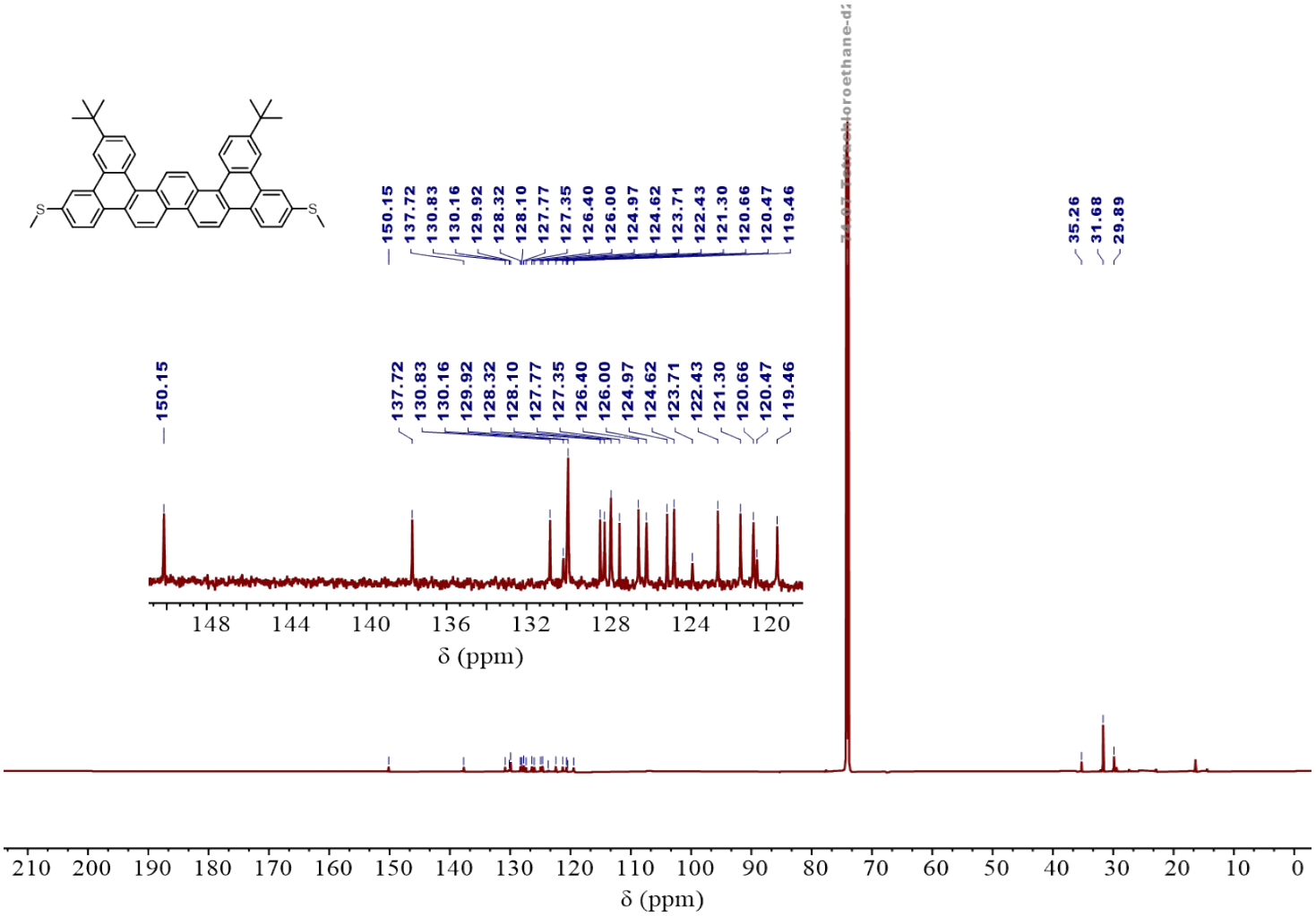

Figure S25. ^{13}C NMR spectrum (151 MHz, Tetrachloroethane-d_2) of **2TP.**

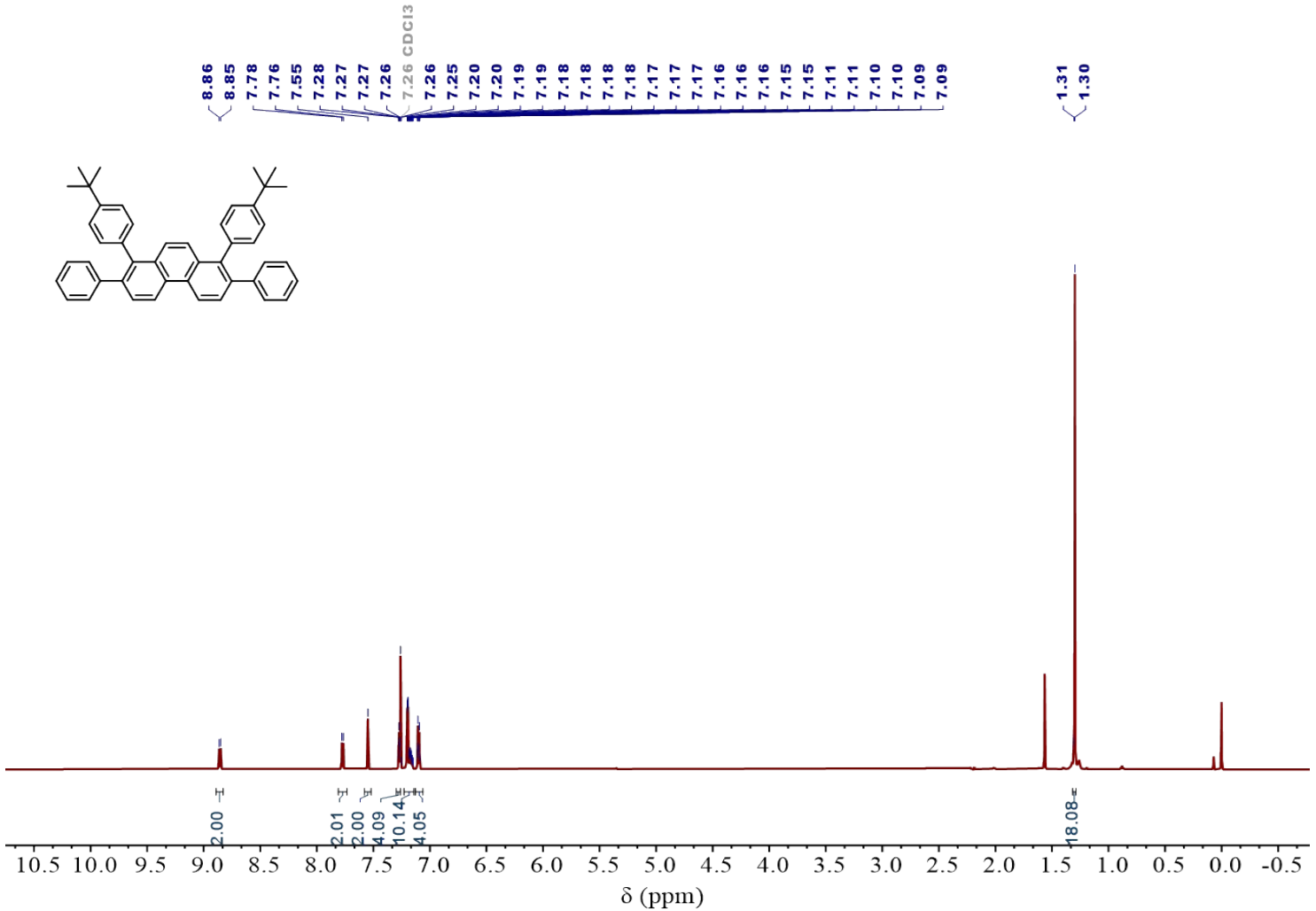

Figure S26. ^{1}H NMR spectrum(600 MHz, Chloroform-d) of **2-Core.**

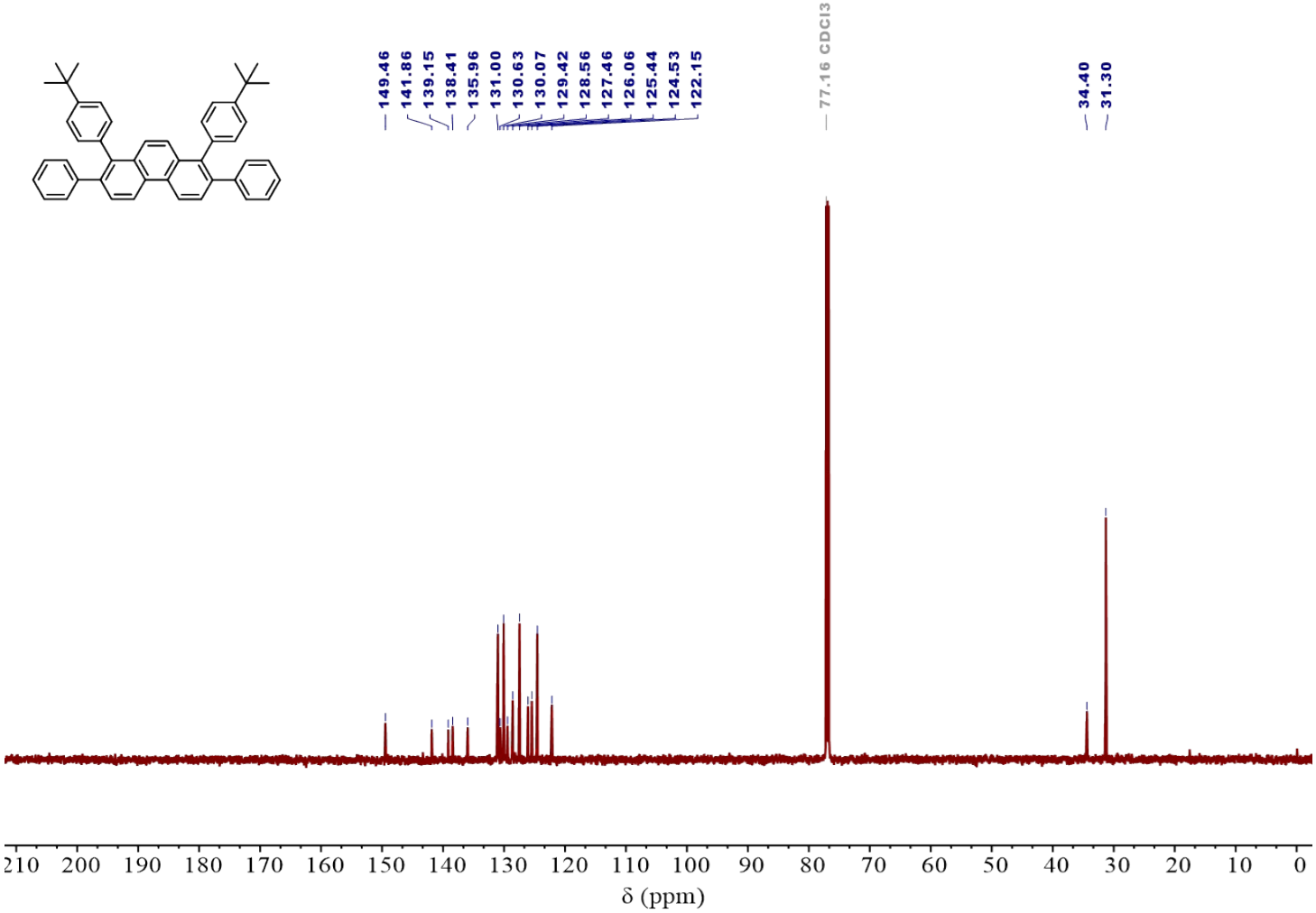

Figure S27. ^{13}C NMR spectrum (151 MHz, Chloroform-d) of **2-Core**.

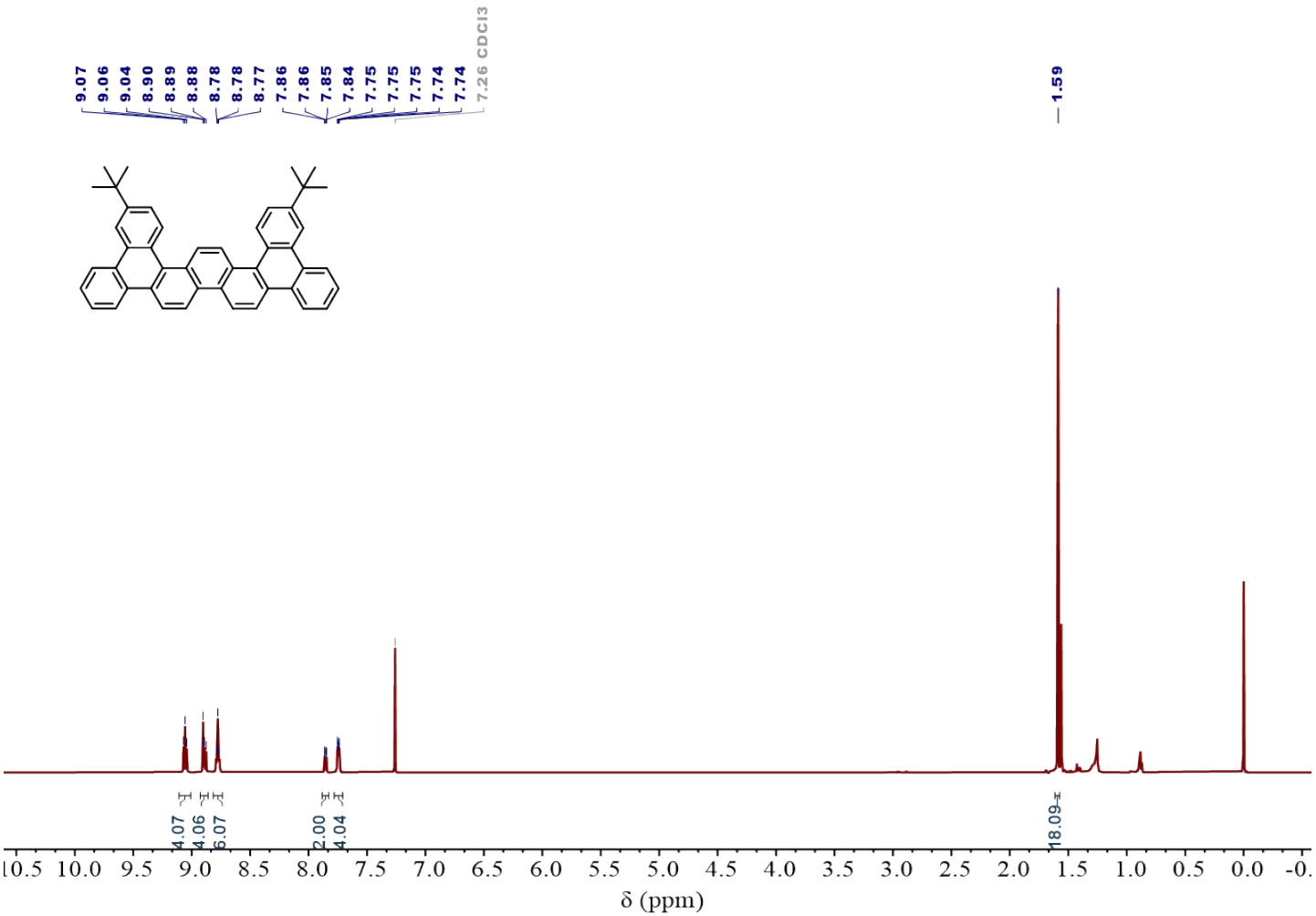

Figure S28. ^{1}H NMR spectrum(600 MHz, Chloroform-d) of **2TP-Core.**

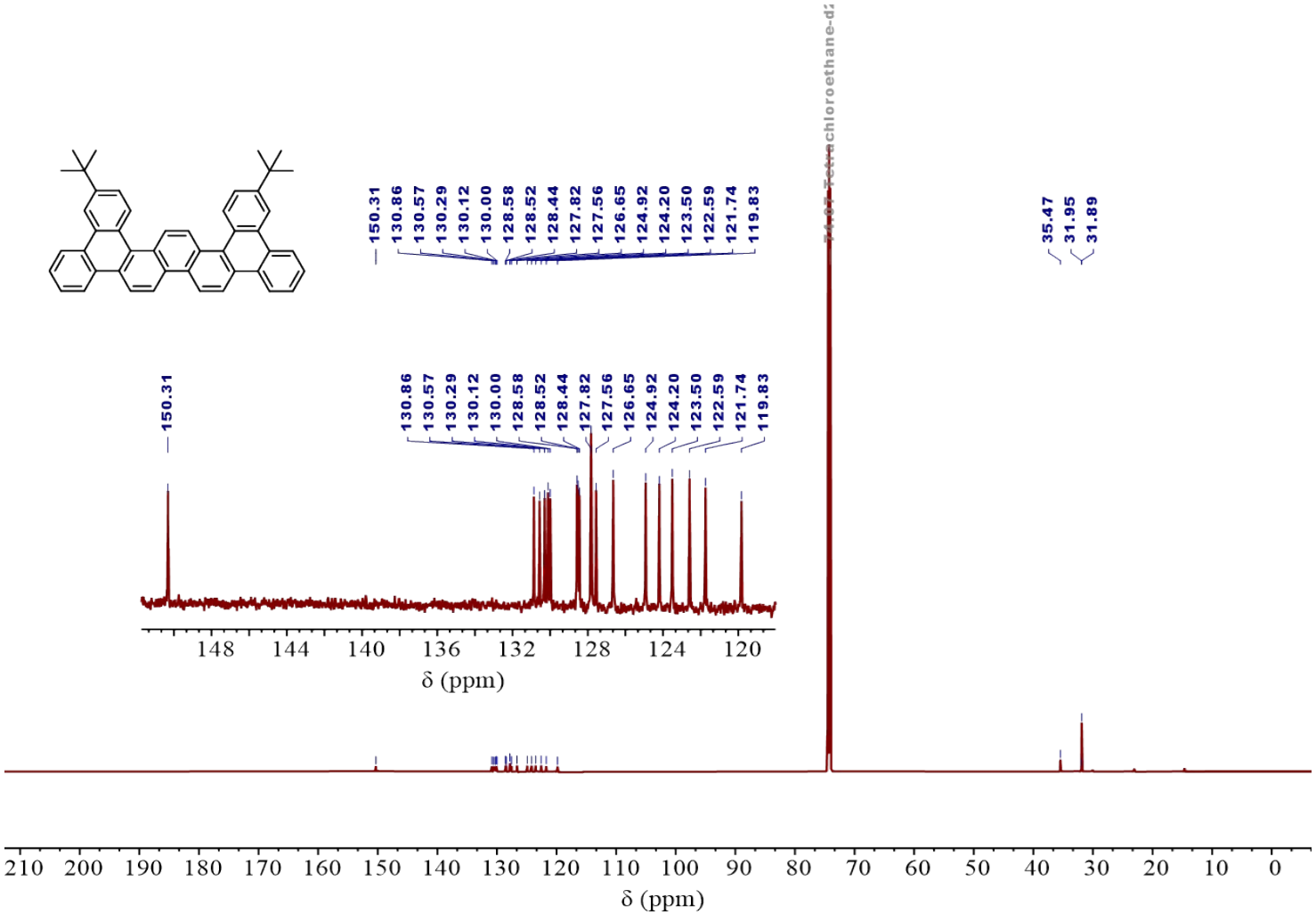

Figure S29. ^{13}C NMR spectrum (151 MHz, Tetrachloroethane-d_2) of **2TP-Core.**

9. Mass spectra

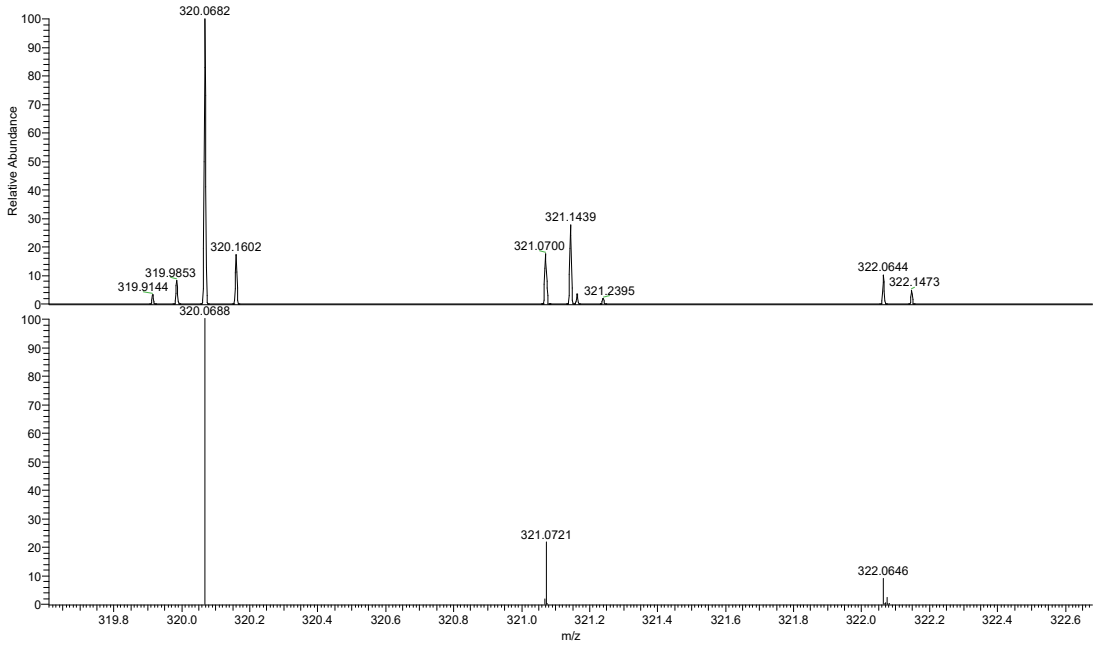

Figure S30. HRMS analysis (ESI) of **TP**
Calculated for $C_{20}H_{16}S_2$ $[M]^+$: 320.0688, found: 320.0682.

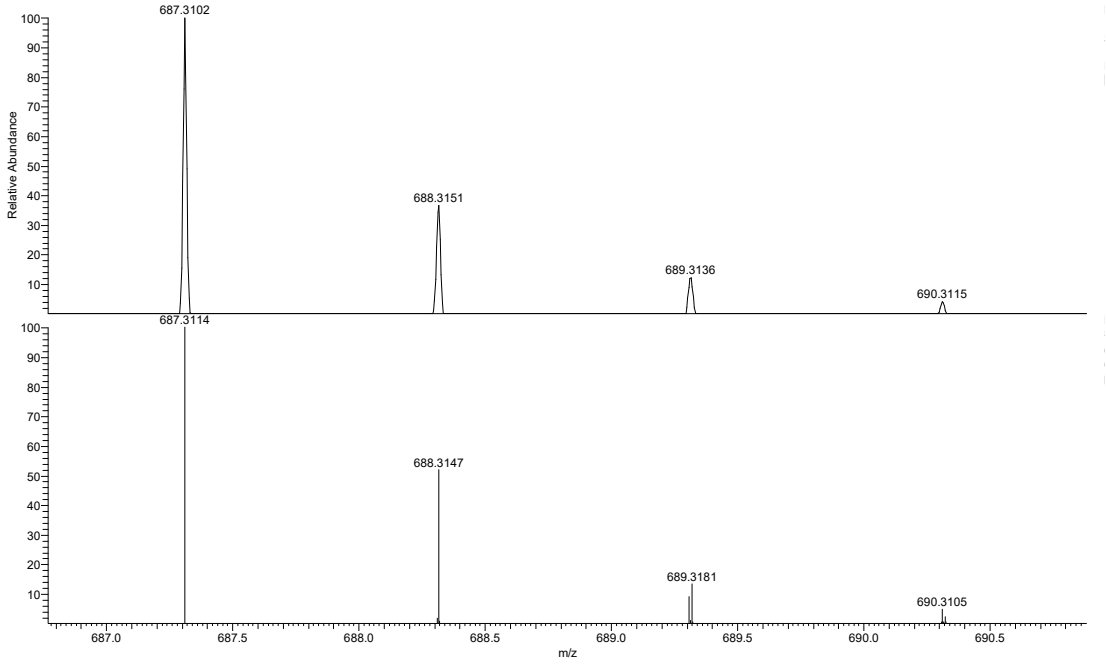

Figure S31. HRMS analysis (ESI) of **2**
Calculated for $C_{48}H_{46}S_2$ $[M+H]^+$: 687.3114, found: 687.3102.

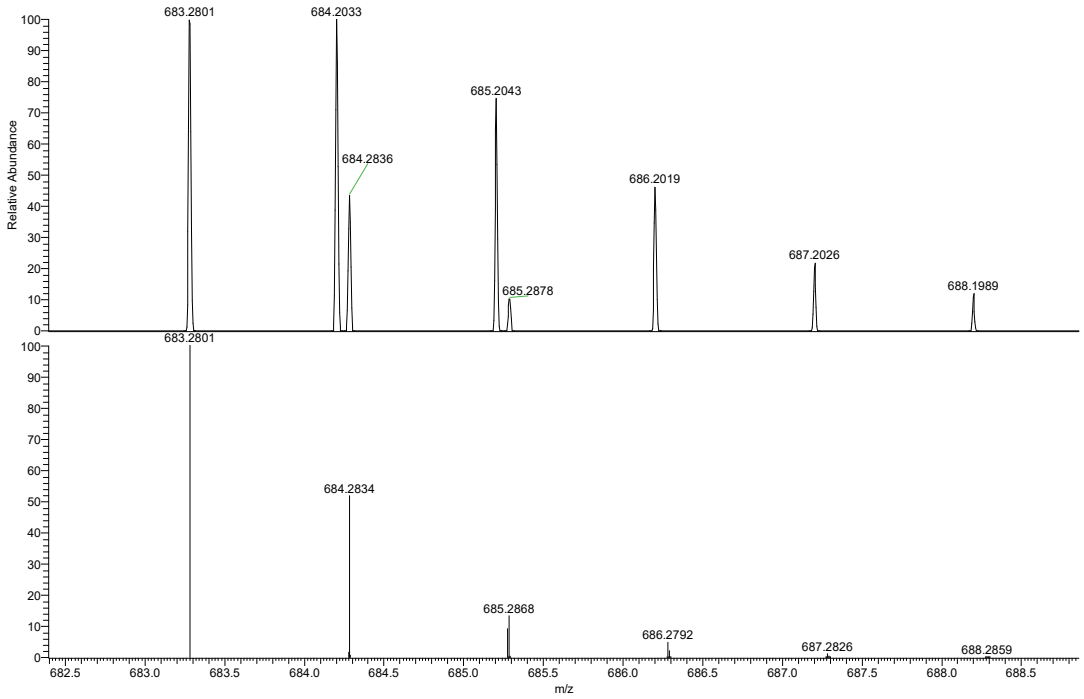

Figure S32. HRMS analysis (ESI) of **2TP**

Calculated for $C_{48}H_{42}S_2$ $[M+H]^+$: 683.2801, found: 683.2801.

10. Cartesian coordinates of optimized structures

TP

C	-1.43897100	0.43897000	-0.10770600
C	-0.72945600	-0.79035100	-0.05704600
C	0.72946900	-0.79033900	0.05704800
C	1.43896600	0.43899200	0.10769200
C	0.70867400	1.71025100	0.05562600
C	-0.70869800	1.71024000	-0.05563900
C	-2.84869700	0.40324800	-0.19226400
C	-3.55563700	-0.78903500	-0.25654900
C	-2.84660700	-2.00383100	-0.23519100
C	-1.47027700	-1.99294500	-0.12429800
C	1.47030800	-1.99292300	0.12430800
C	2.84663900	-2.00378800	0.23519300
C	3.55565100	-0.78898100	0.25653100
C	2.84869400	0.40329100	0.19223600
C	1.37981900	2.95229900	0.11549500
C	0.69784700	4.15441000	0.06009500
C	-0.69790900	4.15439900	-0.06009900
C	-1.37986200	2.95227900	-0.11550200
S	5.33655900	-0.73905000	0.45026700
S	-5.33654500	-0.73913500	-0.45030100
C	5.89012200	-1.73236500	-0.98842400
C	-5.89011000	-1.73225600	0.98852300
H	-3.41823600	1.32379300	-0.19970400
H	-3.37602400	-2.94856900	-0.31441400
H	-0.95684200	-2.94703600	-0.10847200
H	0.95688600	-2.94702100	0.10849500
H	3.37607000	-2.94851800	0.31442200
H	3.41822000	1.32384400	0.19965300
H	2.45855800	2.98084300	0.21086200
H	1.24622000	5.09100800	0.10901100
H	-1.24629600	5.09098900	-0.10901000
H	-2.45860200	2.98080600	-0.21086300
H	6.98286700	-1.74270200	-0.95053200
H	5.52747800	-2.76171000	-0.93142300
H	5.56676500	-1.27508900	-1.92674800
H	-5.52749500	-2.76161800	0.93164200
H	-5.56672300	-1.27487400	1.92678600
H	-6.98285600	-1.74256900	0.95065400

2

C	-5.06775000	-2.15759200	0.06525300
C	-2.85387500	-3.28239000	0.02662300
C	-1.47704000	-3.30737700	0.02894000
C	-0.72460400	-2.11256800	0.02127600
C	-1.43790500	-0.87658200	0.00664600
C	-2.86985700	-0.85929400	0.02945200
C	-3.57890700	-2.06754000	0.03559300
C	0.73350900	-2.11263700	0.01786100
C	1.44668400	-0.87676700	-0.00011500
C	0.68472000	0.33811600	-0.07968400
C	-0.67607300	0.33820100	-0.07653200
C	1.48620800	-3.30735600	0.02190200
C	2.86302000	-3.28214200	0.01317900
C	3.58801700	-2.06715700	0.01901500
C	2.87860400	-0.85921000	0.01590800
C	-3.59142800	0.45172300	0.00358100
C	-3.52831900	1.34268400	1.08216500
C	-4.20628500	2.56355700	1.05402700
C	-4.97151800	2.95125000	-0.05394700
C	-5.02533900	2.05346800	-1.13401500
C	-4.35521600	0.83399400	-1.10914900
C	3.59884500	0.45251100	-0.01205800
C	4.35047300	0.84100700	-1.12618600
C	5.02283900	2.06446400	-1.15450500
C	4.97712100	2.95288300	-0.07207400
C	4.21938100	2.55631600	1.04351200
C	3.54341900	1.33966600	1.07482100
C	5.70798100	4.30761100	-0.06544800
C	6.47418600	4.56628400	-1.37651400
C	4.67955100	5.44811100	0.12375600
C	6.72466100	4.33750100	1.10067800
C	-5.73007900	4.28880300	-0.12407700
C	-5.55003400	5.13225700	1.15226200
C	-5.20830400	5.11443600	-1.32426900
C	-7.24143600	4.01466800	-0.31081400
C	5.07696800	-2.15686300	0.04204800
C	5.74220100	-2.97160000	-0.88740400
C	7.13008000	-3.10896300	-0.86631800
C	7.88998000	-2.45069800	0.10679800
C	7.23270900	-1.65545000	1.05612800
C	5.85030000	-1.50060700	1.01459100
C	-5.83689200	-1.50118800	1.04100900
C	-7.21914000	-1.65616700	1.08833000
C	-7.88028000	-2.45204300	0.14225200
C	-7.12447800	-3.11076200	-0.83375000
C	-5.73677600	-2.97282600	-0.86111900
S	9.66762900	-2.69300700	0.16121100

S	-9.65807300	-2.69252900	0.20490100
C	10.26822300	-0.99883100	-0.20695500
C	-10.25735700	-1.00429200	-0.19224500
H	-3.40600800	-4.21741800	0.05220600
H	-0.97959500	-4.27034100	0.04292500
H	1.21387600	1.28046800	-0.15686500
H	-1.20546700	1.28058300	-0.15096000
H	0.98902900	-4.27042700	0.03808100
H	3.41538300	-4.21710600	0.03599000
H	-2.94403400	1.07710400	1.95980900
H	-4.12772300	3.21350700	1.91867500
H	-5.60168300	2.30765100	-2.01951400
H	-4.42336400	0.16609000	-1.96333300
H	4.41234200	0.17788000	-1.98461700
H	5.58830900	2.31708000	-2.04474200
H	4.15212800	3.20751500	1.91094500
H	2.96671100	1.06843200	1.95571400
H	6.97581900	5.53919900	-1.32489400
H	7.24407900	3.80727100	-1.55614500
H	5.80418000	4.58601100	-2.24356500
H	5.18661200	6.42071500	0.13722300
H	4.12721200	5.34793900	1.06395500
H	3.94937200	5.45678600	-0.69351600
H	7.47261300	3.54426300	0.98842700
H	7.25036500	5.29997700	1.12457000
H	6.23614500	4.20083600	2.07117600
H	-6.10658700	6.07127200	1.05558500
H	-5.92878000	4.61442600	2.04086300
H	-4.49893000	5.38852000	1.32733800
H	-5.74435600	6.06903800	-1.39264400
H	-5.34634800	4.58634500	-2.27352800
H	-4.13961700	5.33173300	-1.21535900
H	-7.64168000	3.43776800	0.53077400
H	-7.79618200	4.95912500	-0.37043300
H	-7.44335700	3.45126300	-1.22778500
H	5.16668000	-3.48488700	-1.65336800
H	7.62823400	-3.72461300	-1.60930500
H	7.80553200	-1.16611700	1.83890400
H	5.36083600	-0.88164300	1.75928600
H	-5.34416900	-0.88177800	1.78315600
H	-7.78914600	-1.16648900	1.87294000
H	-7.62573100	-3.72740500	-1.57381900
H	-5.16435800	-3.48641700	-1.62920600
H	11.36060800	-1.04663000	-0.18701000
H	9.94012100	-0.67418800	-1.19761700
H	9.93165500	-0.28397500	0.54816900
H	-11.34974000	-1.04936500	-0.16637900
H	-9.91543900	-0.27632000	0.54778200
H	-9.93319200	-0.69877400	-1.19025300

2TP

C	2.83104300	-3.09885800	0.77405900
C	1.46704700	-3.07504800	0.89991700
C	0.71603100	-1.92541100	0.54185000
C	1.43497400	-0.76438400	0.13705300
C	2.87743000	-0.73347800	0.21382800
C	3.57172800	-1.94853300	0.39203600
C	-0.73639100	-1.92563400	0.54043000
C	-1.45471800	-0.76471200	0.13523400
C	-0.69229800	0.28583000	-0.46879600
C	0.67313300	0.28602400	-0.46792500
C	-1.48783000	-3.07634600	0.89513800
C	-2.85138200	-3.10062500	0.76641200
C	-3.59198200	-1.94973100	0.38502400
C	-2.89757100	-0.73401500	0.20978600
C	3.65538000	0.50618700	0.15256700
C	3.09444800	1.76932300	0.44256200
C	3.83835100	2.93716400	0.40123000
C	5.20752300	2.91780500	0.08178300
C	5.78364900	1.66702600	-0.12825100
C	5.05983800	0.45961600	-0.07937200
C	-3.67541900	0.50471800	0.14874800
C	-5.07700600	0.45978500	-0.08353300
C	-5.80541300	1.67006000	-0.13499100
C	-5.22885700	2.91561800	0.07647500
C	-3.85567100	2.93278000	0.39898300
C	-3.11167600	1.77019300	0.44053300
C	-5.74951500	-0.83537500	-0.19106800
C	6.07021600	4.19078000	0.00447100
C	-6.02229000	4.23172800	0.01647400
C	-7.11266300	-0.94457200	-0.54364200
C	-7.77027600	-2.16624000	-0.56828900
C	-7.05738400	-3.33308500	-0.23417200
C	-5.72315100	-3.24906200	0.11236400
C	-5.02983200	-2.01624900	0.13276500
C	5.73115800	-0.83734200	-0.18593700
C	7.09322000	-0.94780200	-0.53991700
C	7.75037500	-2.17005900	-0.56303600
C	7.03684100	-3.33541700	-0.22642100
C	5.70260500	-3.24969500	0.12086200
C	5.01052300	-2.01643900	0.14009900
C	5.24701500	5.46818200	0.25859600
C	7.19446500	4.12351200	1.06551200
C	6.70098300	4.29784700	-1.40439200
C	-7.50194700	4.01300000	-0.35099200
C	-5.96612700	4.93247000	1.39517800
C	-5.39179100	5.15568800	-1.05306800
S	-9.47841100	-2.23445400	-1.10960600

S	9.45822900	-2.24004300	-1.10499500
C	10.27552700	-2.95690900	0.37231000
C	-10.29501000	-2.95688900	0.36532700
H	3.35105200	-4.01990300	1.00952100
H	0.96653700	-3.97352300	1.24061800
H	-1.21161300	1.06787900	-1.00912900
H	1.19309400	1.06836600	-1.00715900
H	-0.98752600	-3.97532000	1.23482400
H	-3.37148400	-4.02231900	0.99911300
H	2.05964100	1.83304600	0.75395900
H	3.34298100	3.87083300	0.64300300
H	6.85197300	1.62132900	-0.30160700
H	-6.87050000	1.61904800	-0.31214100
H	-3.36520200	3.87077000	0.64333300
H	-2.07720000	1.83224500	0.75329200
H	-7.67808400	-0.06099600	-0.81288700
H	-7.54664000	-4.30170000	-0.27522800
H	-5.19520200	-4.17053000	0.32826900
H	7.65856100	-0.06480200	-0.81141500
H	7.52517900	-4.30455600	-0.26611500
H	5.17414200	-4.17046700	0.33841900
H	5.89556600	6.34734500	0.17411700
H	4.43729600	5.58329900	-0.47100700
H	4.80778700	5.47922000	1.26265300
H	7.81592100	5.02622100	1.01941700
H	7.85065600	3.26047900	0.91194200
H	6.77623500	4.04968600	2.07582900
H	5.92656300	4.35790600	-2.17755800
H	7.32370600	5.19800600	-1.47575800
H	7.33507300	3.43522100	-1.63410100
H	-8.01598100	4.97949300	-0.39967900
H	-7.61256200	3.53043900	-1.32874100
H	-8.02293600	3.40155500	0.39457300
H	-6.52093000	5.87815900	1.36413400
H	-4.93850900	5.16025800	1.69717800
H	-6.41148800	4.30224700	2.17332800
H	-5.42966700	4.69036700	-2.04459500
H	-5.93536200	6.10707900	-1.10261800
H	-4.34381300	5.38215100	-0.83017700
H	11.33777700	-3.03945900	0.12626100
H	10.15660700	-2.30416700	1.24067600
H	9.88912500	-3.95337900	0.60077500
H	-11.35732800	-3.03875800	0.11933900
H	-9.90839200	-3.95411700	0.59011300
H	-10.17595800	-2.30726500	1.23601400

11. References

(1) Li, Y.; Yagi, A.; Itami, K. Synthesis of sterically hindered 4,5-diarylphenanthrenes via acid-catalyzed bisannulation of benzenediacetaldehydes with alkynes. *Chemical Science* **2019**, *10* (21), 5470-5475.
(2) Röse, P.; Emge, S.; König, C. A.; Hilt, G. Efficient Oxidative Coupling of Arenes via Electrochemical Regeneration of 2,3 - Dichloro - 5,6 - dicyano - 1,4 - benzoquinone (DDQ) under Mild Reaction Conditions. *Adv. Synth. Catal.* **2017**, *359* (8), 1359-1372.
(3) Würth, C.; Grabolle, M.; Pauli, J.; Spieles, M.; Resch-Genger, U. Relative and absolute determination of fluorescence quantum yields of transparent samples. *Nature Protocols* **2013**, *8* (8), 1535-1550.
(4) Farney, E. P.; Chapman, S. J.; Swords, W. B.; Torelli, M. D.; Hamers, R. J.; Yoon, T. P. Discovery and Elucidation of Counteranion Dependence in Photoredox Catalysis. *J. Am. Chem. Soc.* **2019**, *141* (15), 6385-6391.
(5) Hong, W.; Manrique, D. Z.; Moreno-García, P.; Gulcur, M.; Mishchenko, A.; Lambert, C. J.; Bryce, M. R.; Wandlowski, T. Single Molecular Conductance of Tolanes: Experimental and Theoretical Study on the Junction Evolution Dependent on the Anchoring Group. *J. Am. Chem. Soc.* **2012**, *134* (4), 2292-2304.
(6) Venkataraman, L.; Klare, J. E.; Nuckolls, C.; Hybertsen, M. S.; Steigerwald, M. L. Dependence of single-molecule junction conductance on molecular conformation. *Nature* **2006**, *442* (7105), 904-907.
(7) Xie, Z.; Bâldea, I.; Frisbie, C. D. Energy Level Alignment in Molecular Tunnel Junctions by Transport and Spectroscopy: Self-Consistency for the Case of Alkyl Thiols and Dithiols on Ag, Au, and Pt Electrodes. *J. Am. Chem. Soc.* **2019**, *141* (45), 18182-18192.
(8) Xie, Z.; Bâldea, I.; Frisbie, C. D. Determination of Energy-Level Alignment in Molecular Tunnel Junctions by Transport and Spectroscopy: Self-Consistency for the Case of Oligophenylene Thiols and Dithiols on Ag, Au, and Pt Electrodes. *J. Am. Chem. Soc.* **2019**, *141* (8), 3670-3681.
(9) *Gaussian 16 Rev. C.01*; Wallingford, CT, 2016. (accessed.
(10) Chai, J.-D.; Head-Gordon, M. Long-range corrected hybrid density functionals with damped atom–atom dispersion corrections. *PCCP* **2008**, *10* (44), 6615-6620.
(11) Tomasi, J.; Mennucci, B.; Cammi, R. Quantum Mechanical Continuum Solvation Models. *Chem. Rev.* **2005**, *105* (8), 2999-3094.
(12) Neese, F. Software update: The ORCA program system—Version 5.0. *WIREs Computational Molecular Science* **2022**, *12* (5), e1606.
(13) Neese, F. Software update: the ORCA program system, version 4.0.

WIREs Computational Molecular Science **2018**, *8* (1), e1327.
(14) Neese, F.; Wennmohs, F.; Becker, U.; Riplinger, C. The ORCA quantum chemistry program package. *J Chem Phys* **2020**, *152* (22), 224108.
(15) Neese, F. The ORCA program system. *WIREs Computational Molecular Science* **2012**, *2* (1), 73-78.
(16) Neese, F.; Wennmohs, F.; Hansen, A.; Becker, U. Efficient, approximate and parallel Hartree–Fock and hybrid DFT calculations. A 'chain-of-spheres' algorithm for the Hartree–Fock exchange. *Chem. Phys.* **2009**, *356* (1), 98-109.
(17) Mardirossian, N.; Head-Gordon, M. ωB97M-V: A combinatorially optimized, range-separated hybrid, meta-GGA density functional with VV10 nonlocal correlation. *J. Chem. Phys.* **2016**, *144* (21).
(18) Weigend, F.; Ahlrichs, R. Balanced basis sets of split valence, triple zeta valence and quadruple zeta valence quality for H to Rn: Design and assessment of accuracy. *PCCP* **2005**, *7* (18), 3297-3305.
(19) Weigend, F. Accurate Coulomb-fitting basis sets for H to Rn. *PCCP* **2006**, *8* (9), 1057-1065.
(20) Marenich, A. V.; Cramer, C. J.; Truhlar, D. G. Universal Solvation Model Based on Solute Electron Density and on a Continuum Model of the Solvent Defined by the Bulk Dielectric Constant and Atomic Surface Tensions. *The Journal of Physical Chemistry B* **2009**, *113* (18), 6378-6396.
(21) Kruse, H.; Grimme, S. A geometrical correction for the inter- and intra-molecular basis set superposition error in Hartree-Fock and density functional theory calculations for large systems. *J. Chem. Phys.* **2012**, *136* (15).
(22) Grimme, S. Supramolecular Binding Thermodynamics by Dispersion-Corrected Density Functional Theory. *Chemistry – A European Journal* **2012**, *18* (32), 9955-9964.
(23) Lu, T.; Chen, Q. Shermo: A general code for calculating molecular thermochemistry properties. *Computational and Theoretical Chemistry* **2021**, *1200*, 113249.
(24) Humphrey, W.; Dalke, A.; Schulten, K. VMD: Visual molecular dynamics. *J. Mol. Graphics* **1996**, *14* (1), 33-38.
(25) Stephens, P. J.; Devlin, F. J.; Chabalowski, C. F.; Frisch, M. J. Ab Initio Calculation of Vibrational Absorption and Circular Dichroism Spectra Using Density Functional Force Fields. *J. Phys. Chem.* **1994**, *98* (45), 11623-11627.
(26) Grimme, S.; Ehrlich, S.; Goerigk, L. Effect of the damping function in dispersion corrected density functional theory. *J. Comput. Chem.* **2011**, *32* (7), 1456-1465.
(27) Adamo, C.; Barone, V. Toward reliable density functional methods without adjustable parameters: The PBE0 model. *J. Chem. Phys.* **1999**, *110* (13), 6158-6170.
(28) Yanai, T.; Tew, D. P.; Handy, N. C. A new hybrid exchange–correlation functional using the Coulomb-attenuating method (CAM-B3LYP). *Chem. Phys.*

Lett. **2004**, *393* (1), 51-57.
(29) Zhao, Y.; Truhlar, D. G. The M06 suite of density functionals for main group thermochemistry, thermochemical kinetics, noncovalent interactions, excited states, and transition elements: two new functionals and systematic testing of four M06-class functionals and 12 other functionals. *Theor. Chem. Acc.* **2008**, *120* (1), 215-241.
(30) Lu, T.; Chen, F. Multiwfn: A multifunctional wavefunction analyzer. *J. Comput. Chem.* **2012**, *33* (5), 580-592.
(31) Wu, S.-D.; Liu, S.-T.; Cai, Z.-M.; Sun, B.; Liu, X.-D.; Shi, L.-Y.-Y.; Lambert, C. J.; Zhang, H.-L. Breaking Interference-Driven Reversal Currents to Boost Single-Molecule Conductance. *Angew. Chem. Int. Ed. n/a* (n/a), e202520318.